Modeling particle nucleation and growth over northern California during the 2010 CARES campaign

A. Lupascu[1], R. Easter[1], R. Zaveri[1], M. Shrivastava[1], M. Pekour[1], J. Tomlinson[1], Q. Yang[1], H. Matsui[2,3], A. Hodzic[4], Q. Zhang[5], and J. D. Fast[1]

[1]{Pacific Northwest National Laboratory, Richland, Washington, USA}

[2]{Graduate School of Environmental Studies, Nagoya University, Nagoya, Japan}

[3]{Department of Environmental Geochemical Cycle Research, Japan Agency for Marine-Earth Science and Technology, Yokohama, Japan}

[4]{National Center for Atmospheric Research, Boulder, Colorado, USA}

[5]{Department of Environmental Toxicology, University of California – Davis, Davis, California, USA}

Correspondence to: J. D. Fast (Jerome.Fast@pnnl.gov)

Abstract

Accurate representation of the aerosol lifecycle requires adequate modeling of the particle number concentration and size distribution in addition to their mass, which is often the focus of aerosol modeling studies. This paper compares particle number concentrations and size distributions as predicted by three empirical nucleation parameterizations in the Weather Research and Forecast coupled with chemistry (WRF-Chem) regional model using 20 discrete size bins ranging from 1 nm to 10 μm. Two of the parameterizations are based on H_2SO_4 while one is based on both H_2SO_4 and organic vapors. Budget diagnostic terms for transport, dry deposition, emissions, condensational growth, nucleation, and coagulation of aerosol particles have been added to the model and are used to analyze the differences in how the new particle formation parameterizations influence the evolving aerosol size distribution. The simulations are evaluated using measurements collected at surface sites and from a research aircraft

during the Carbonaceous Aerosol and Radiative Effects Study (CARES) conducted in the vicinity of Sacramento, California.

While all three parameterizations captured the temporal variation of the size distribution during observed nucleation events as well as the spatial variability in aerosol number, all overestimated by up to a factor of 2.5 the total particle number concentration for particle diameters greater than 10 nm. Using the budget diagnostic terms, we demonstrate that the combined H_2SO_4 and low-volatility organic vapors parameterization leads to a different diurnal variability of new particle formation and growth to larger sizes compared to the parameterizations based on only H_2SO_4. At the CARES urban ground site, peak nucleation rates are predicted to occur around 1200 Pacific (local) standard time (PST) for the H_2SO_4 parameterizations, whereas the highest rates were predicted at 0800 and 1600 PST when low-volatility organic gases are included in the parameterization. This can be explained by higher anthropogenic emissions of organic vapors at these times as well as lower boundary layer heights that reduce vertical mixing. The higher nucleation rates in the H_2SO_4-organic parameterization at these times were largely offset by losses due to coagulation. Despite the different budget terms for ultrafine particles, the 10 – 40 nm diameter particle number concentrations from all three parameterizations increased from 1000 to 1400 PST and then decreased later in the afternoon, consistent with changes in the observed size and number distribution. We found that newly formed particles could explain up to 20 – 30 % of predicted cloud condensation nuclei at 0.5% supersaturation, depending on location and the specific nucleation parameterization. A sensitivity simulation using 12 discrete size bins ranging from 1 nm to 10 μm diameter gave a reasonable estimate of particle number and size distribution compared to the 20 size bin simulation, while reducing the associated computational cost by ~ 36 %.

1 Introduction

Aerosol particles are ubiquitous in the atmosphere and are important for their potential climate impact and role in atmospheric chemistry. They absorb and scatter solar radiation, act as cloud condensation nuclei (CCN) and ice nuclei (IN), and induce an

overall cooling effect (IPCC, 2007; 2013). They are classified depending on their origin and source as primary or secondary particles. Primary particles originate from natural sources, such as dust and sea-salt, as well as anthropogenic sources, such as combustion. Secondary particles are formed through gas-to-particle partitioning processes. The formation of secondary aerosol particles and their subsequent growth has been observed in rural (Place et al., 2010, Ziemba et al., 2006), urban (Betha et al., 2013, Matsui et al., 2011, Jeong et al., 2004), marine (Hoppel et al., 1994, O'Dowd and Hoffmann, 2005), and high altitude (Venzac et al., 2009, Boulon et al., 2011, Cui et al., 2014) environments. Makkonen et al., (2009), Spracklen et al. (2006, 2008, 2010) and many others have shown that secondary particle formation contributes to cloud condensation nuclei (CCN) and subsequently influence cloud droplet number concentrations and other cloud processes.

Sulfuric acid gas (H_2SO_4) plays an important role in the formation of small secondary aerosol particles, due to its very low vapor pressure. Recent studies showed that H_2SO_4 alone cannot explain the abundance of new particles in the troposphere (Merikanto et al., 2007, Kirkby, et al. 2011, Schobesberger et al., 2013). Thus, several mechanisms have been proposed to describe the formation of new particles in the troposphere: the binary homogeneous mechanism (BHN) involving H_2SO_4-H_2O (Wexler et al. 1994, McMurry, 1980, McMurry et al., 2000, Kulmala et al., 1998, Vehkamaki et al., 2002), the ternary nucleation (TN) mechanism involving H_2SO_4-H_2O-ammonia (NH_3) (Napari et al., 2002, Merikanto et al., 2007), the ion induced nucleation mechanism (IIN) (Turco et al, 1998, Yu and Turco, 2000, 2001, Yu et al., 2008, Kazil et al., 2008), empirical particle formation mechanisms involving H_2SO_4 (Kulmala et al., 2006; Sihto et al., 2006; Riipinen et al., 2007; Kuang et al., 2008), and the combined organic and sulfuric acid (kinetic-type) empirical mechanism (ORG) (Metzger et al. 2010, Paasonen et al. 2010, Schobesberger et al., 2013, Ehn et al., 2014, Riccobono et al. 2014). In the empirical particle formation mechanisms, the nucleation rate is proportional to the H_2SO_4 concentration to the power of 1 to 2; the activation mechanism (ACT) (Kulmala et al., 2006) uses a power of one while the kinetic nucleation mechanism (KIN) (McMurry and Friedlander, 1979, Kuang et al., 2008) uses a power of two. Due to its dependency on temperature, the BHN mechanism produces new particles in the upper and free

troposphere (e.g. Spracklen et al., 2005), while the use of state-of-the-science empirical parameterizations like ACT, KIN or ORG lead to better agreement between modeled and observed total number concentration in the boundary layer (i.e., Zhang et al., 2010a, Redington et al. 2011).

In spite of recent advancements, aerosol nucleation and growth processes are not yet completely understood mainly due to limited coincident measurements of aerosol nucleation precursors (such as H_2SO_4, NH_3, and organic acids), and the size, composition, and concentration of newly formed nanometer-sized particles. During the Cosmics Leaving OUtdoor Droplets (CLOUD) experiment, Kirby et al. (2011) showed that ternary nucleation involving H_2SO_4-H_2O-NH_3, with and without ions, did not explain the observed boundary layer nucleation, suggesting that organic vapors participated in atmospheric nucleation. Several studies (i.e., Kuang et al., 2010, 2012, Smith et al., 2008) show that in many environments, H_2SO_4 accounts for less than half of the total growth of the particles. Setyan et al. (2012) suggested that organic vapors and, to a lesser extent, H_2SO_4 play key roles in new particle growth. Recent studies studies (e.g. Ehn et al., 2014, Jokinen et al., 2015) further demonstrate that the organic vapors with extremely low and low-volatility can enhance, or even dominate, the formation and growth of aerosol particles. Still, the role of organic vapors in particle nucleation and subsequent growth processes is quantitatively very uncertain.

Several studies have been conducted to assess how the choice of nucleation scheme affects simulated particle number concentration (PNC) and their size distribution using global and regional models. For example, Jung et al. (2008) analyzed the impact of different nucleation parameterizations on the modeled size distribution predicted by the Dynamic Model for Aerosol Nucleation (DMAN) and its ability to reproduce the nucleation events and non-events observed during the Pittsburgh Air Quality Study (PAQS) conducted between July 2001 and September 2002. They showed that most of the nucleation schemes included in their study had difficulty reproducing the observed events, except for the ternary mechanism of Napari et al. (2002) that predicts the occurrence of the events during the analyzed period. The empirical particle formation mechanism (Sihto et al., 2006) performed well on 70% of the analyzed days, but still it predicted nucleation events on days when nucleation was not observed. The BHN

mechanism of Vehkamaki et al. (2002) did not reproduce any observed nucleation events, and the scaling of the nucleation rate by a correction factor of 10^{10} led to a predicted event on a non-event day. Zhang et al., (2010a) quantified the impact of 11 nucleation schemes on predicted PNC, volume, and surface area using the U.S. Environmental Protection Agency Community Multiscale Air Quality (CMAQ) modeling system version 4.4. They concluded that, although all the parameterizations underpredicted the total PNC (by a factor of 1.3 to 14.5), the ACT empirical formation mechanism (Sihto et al., 2006) led to the best prediction, while the least reliable prediction was given by the Merikanto et al. (2007) TN parameterization. Using the Global Model of Aerosol Processes (GLOMAP), Reddington et al. (2011) showed the use of ACT, KIN and ORG parameterizations led to underpredictions spanning from -53% to -11% of total PNC in the boundary layer for continental European monitoring station. In contrast, Jung et al. (2010) found that the PMCAMx-UF model using the TN nucleation parameterization (Napari et al., 2002), with the nucleation rate corrected using a nucleation tuner equal to 10^{-5}, overpredicted by 22% the total number concentration of particles having a diameter larger than 3 nm, while this overprediction was greater than 49% for particles having a diameter larger than 10 nm. Westervelt et al. (2013) have the Goddard Earth Observing System global chemical transport model (GEOS-Chem) coupled to the TwO-Moment Aerosol Sectional (TOMAS) scheme to evaluate the performance of a ternary nucleation parameterization (Napari et al., 2002, with an added 10^{-5} nucleation tuning factor) and the ACT nucleation parameterization (Sihto et al., 2006). Using metrics such as nucleation rate, growth rate, condensation and coagulation sink, survival probability, and CCN formation they investigated the limitation of nucleation and SOA parameterizations at five locations in the various location and environments showing that, although the model gave reasonable results on average, the largest discrepancies between model and measurements were obtained using the ACT parameterization at the urban sites (up to a factor of 5 for the formation rate of 3 nm particles). Yu (2011), Riipinen et al., (2011), Pierce et al., (2011), and Patoulias et al., (2015) studied the impact of secondary organic vapor condensation and the average saturation concentration of these vapors on formation of new particles and their growth to larger sizes. They found that the condensation of these vapors can contribute to new particle formation as well to the growth of these

ultrafine particles. A recent study of Yu et al. (2015) compared the Ion-Mediation Nucleation (IMN) mechanism and the organics mediated mechanism derived from the Cosmics Leaving Outdoor Droplets (CLOUD) chamber experiment (Riccobono et al., 2014) for several locations in North-America. It was shown that the frequency of nucleation and the intensity of NPF predicted by the organics-mediated mechanism was too high, while IMN parameterization was closer to the observed values, especially during the spring. That study suggested that the spatial and temporal differences in the behavior of the two nucleation parameterizations could be related to differences in the predicted aerosol first indirect radiative forcing, a lower concentration of organic compounds in the atmosphere compared to those used in chamber studies and the temperature influence on atmospheric nucleation rate compared to the derived empirical coefficient at a 278 K temperature and 39% relative humidity.

The aim of this study is to determine the performance of several new particle formation parameterizations implemented in the chemistry version of the Weather Research and Forecasting model (WRF-Chem) and investigate how differences in the parameterization formulations affect simulated spatial and temporal variations in boundary layer particle number concentrations during the Carbonaceous Aerosol and Radiative Effects Study (CARES) (Zaveri et al., 2012). The principal objectives of CARES were to examine the interaction between anthropogenic and biogenic precursors associated with secondary organic aerosol formation, the evolving mixing state of secondary organic and black carbon aerosols, and the impact of aerosols on optical and CCN activation properties. A complete overview of the research objectives and the ground and aircraft measurements collected during the CARES campaign is given by Zaveri et al., (2012). Although the primary objectives of the campaign did not include examining the formation of new particles, measurements of particle number concentration and size distribution showed that new particle formation events frequently occurred in the vicinity of Sacramento and over the western Sierra foothills. This environment is influenced by the SO_2 emissions originating from oil refineries located in the vicinity of the Carquinez Strait and the San Francisco Bay area. Setyan et al., (2014) showed that on days with new particle formation events during CARES, the concentration of organics and sulfate significantly increased in particles in the Aitken mode and that the concentrations of species

representative of urban emissions together with the photo-oxidation products of biogenic volatile organic compounds (VOCs) and the biogenically influenced secondary organic aerosols (SOA) were on average 50% higher during the event days compared to the non-event days. These findings provide means to test several particle formation mechanisms that include the effect of sulfuric acid alone or combined effect of sulfuric acid and organic vapors, in addition to the BHN mechanism currently available in WRF-Chem.

The CARES measurements are described in Section 2. Key features and details of the WRF-Chem model and the simulations are described in Section 3. Section 4 presents the simulated evolution of the particle number concentration compared with surface and aircraft measurements collected on days in which new particle formation and growth events did and did not occur, and Section 5 summarizes the results.

2 Measurements

During the CARES campaign ground measurements were acquired at two sites in northern California: one in Sacramento (38.645^{o} N, 121.34^{o} W, ~30 m a.s.l.) and the other in Cool (38.89^{o} N, 120.97^{o} W, ~450 m a.s.l.), a small town located about 40 km northeast of Sacramento. Following Zaveri at al., (2010), we will refer to the Sacramento and Cool sites as "T0" and "T1", respectively. Aerosol particle size measurements at both sites were carried out using a Scanning Mobility Particle Sizer (SMPS) to measure the particle the size distribution from 10 nm to 700 nm. Due to the lack of measurements in the 1-10 nm size range, the formation of new particles was not observed. Therefore, in the forthcoming discussion, following Setyan's et al. (2014) terminology, instead of "nucleation" and "new particle formation", we will use the term "new particle formation and growth event" (NPE). While the SMPS does not capture the initiation of NPEs, Zaveri et al. (2010) and Setyan et al. (2014) showed that the growth of small particles frequently occurred during the campaign. The CCN concentration at multiple supersaturations (0.07 to 0.5%) was measured at both sites using Droplet Measurement Technologies CCN Counters (Model 200-013 and 100-081) (Zaveri et al., 2012). In addition to ground-based measurements, the ARM Aerial Facility Gulfstream-1 (G-1) research aircraft sampled on 14 days during the CARES campaign. Aerosol

instrumentation on the G-1 aircraft included CPC-3025 and CPC-3010 condensation particle counters (Sem, 2002) that measured particle number concentrations for particle diameters greater than 3 and 10 nm, respectively.

3 Model

In this study, the WRF-Chem model version 3.5 was used (Grell et al., 2005, Fast et al., 2006) to simulate new particle formation events and their impact on aerosol size distributions and CCN concentrations. The model domain covers the area between 32.2 to 42.7^{O} N, and 127.5 to 113.4^{O} W, which encompassed all of California and Nevada and extended about 400 km into the Pacific (west of San Francisco), using a 4-km grid spacing and 65 vertically-stretched layers from the ground up to 50 hPa. The physics options used for this study include the Morrison double-moment microphysics scheme (Morrison et al., 2009), the Kain-Fritsch cumulus parameterization (Kain, 2004), the Rapid Radiative Transfer Model (Iacono et al., 2008) for longwave and shortwave radiation, the Mellor-Yamada-Janjic boundary-layer parameterization (Janjic, 2001), and the Monin-Obukhov scheme for the surface layer.

Gas-phase chemistry is simulated using the SAPRC-99 mechanism (Carter, 2000). Aerosol lifecycle processes are represented by the Model for Simulating Aerosol Interactions and Chemistry (MOSAIC) (Zaveri et al., 2008), which has been used in numerous aerosol modeling studies (i.e. Cui et al., 2014, Ritter et al., 2013, Archer-Nicholls et al., 2014). Aerosol species in MOSAIC included sulfate, nitrate, ammonium, sodium, chloride, calcium, carbonate, other inorganics (i.e. dust), methanesulfonate, elemental carbon, primary organic aerosols (POA), and aerosol water (Zaveri et al., 2008). Secondary organic aerosols (SOA) are represented by the simplified volatility basis-set (VBS) approach of Shrivastava et al. (2011), with additional updates for biogenic SOA yields (Shrivastava et al, 2015, Shrivastava et al. 2015, in preparation). The VBS approach treats traditional and non-traditional SOA species and precursor gases that partition between particle and gas phases. Traditional SOA precursors derive from oxidation of anthropogenic (e.g., aromatics) and biogenic (e.g., isoprene and terpenes) primary gases, and these are represented with 4 volatility bins having saturation vapor

concentrations (C*) of 0.1, 1, 10 and 100 μg m^{-3} (at 298 K), with effective SOA yields derived from fitting smog chamber data and thus representing the first few generations of oxidation. Non-traditional SOA precursor gases derive from the oxidation of semi- and intermediate volatility primary gases that are emitted during fossil and bio-fuel combustion and biomass burning; these are represented with 2 volatility bins having C* of 0.001 and 10^6 μg m^{-3}. The SOA mass predicted by the simplified 2-species VBS approach is aligned to a complex multi-generational 9-species VBS approach (reducing reaction rate with OH radicals to compensate for the large volatility decrease of organic vapors, as described by Shrivastava et al. 2011). The C* of the lowest volatility bin was reduced from the 0.01 μg m^{-3} used in Shrivastava et al. (2011) to 0.001 μg m^{-3} for this study to allow condensation onto 1 nm particles, for which the Kelvin effect is very large.

Initial and boundary conditions for the chemical species in our simulations, including the mass and number size distribution of primary aerosol species, are taken from the MOZART-4 global chemistry-transport model (Emmons et al., 2010). We reduced the initial and boundary conditions of aerosol concentrations from MOZART-4 by 50% since Fast et al. (2014) found that long-range transport was likely over-estimated when comparing simulated values to aerosol optical depth and extinction profile measurements.

Biogenic trace gas emissions are calculated online using the MEGAN model (Guenther et al., 2006). Anthropogenic emissions are obtained from the California Air Resources Board (CARB) 2010 project emissions available at http://www.arb.ca.gov/app/emsinv/fcemssumcat2009.php. The lognormal size distribution of emitted anthropogenic primary particles uses a geometrical mean diameter of 50 nm and a standard deviation of 2 (Cui et al., 2014). To avoid an artificial increase of 1 nm particles, primary aerosol emissions for particles smaller than 10 nm are not considered. Mineral dust and sea salt emissions are calculated on line (Shaw et al., 2008).

In the public release of WRF-Chem, MOSAIC uses a sectional framework where the aerosol size distribution is divided into 4 or 8 discrete size bins spanning 39 nm to 10 μm diameter. However, these bins do not capture the freshly nucleated particles that have diameters of a few nanometers. Recently, Matsui et al., (2011, 2013) and Cui at al., (2014) added a new sectional framework option for MOSAIC in WRF-Chem that uses 20

bins to represent nucleation and particle growth in the range of 1 nm to 10 μm, and a state-of-the-science empirical cluster activation (ACT) theory parameterization (Kulmala et al., 2006, Sihto et al., 2006). They compared new particle formation (NPF) and particle number concentrations predicted by that approach with land- and aircraft-based measurements. In Matsui et al., (2011), the use of empirical activation type nucleation inside WRF-Chem generally reproduced the number of observed event and non-event days for a measurement site located ~50 km south of Beijing; however, the modeled SO_2 concentration was overestimated by a factor of 6 for this location. Matsui et al. (2013) applied the same approach for another case using several stations located in Korea and Japan. In that study, the simulated average number concentration for particles having a diameter greater than 10 nm (CN10) was overestimated within a factor of 2, while the temporal variation of CN10 was not well reproduced. Cui et al. (2014) showed that the use of the ACT parameterization combined with an improved treatment of SOA formation from biogenic emissions at a forest site in Colorado led to a more accurate simulation of aerosol particles in the 4–100 nm size range compared with the default WRF-Chem model, including onset times, number concentrations, and number mean diameters.

For this study, we performed simulations using the 20 size bin framework (Matsui et al., 2011, 2013; Cui at al., 2014) with 5 different nucleation parameterizations: two based on classical binary homogeneous nucleation theory (Wexler et al., 1994 and Vehkamaki et al., 2002) and 3 newer empirical parameterizations. The Wexler parameterization is the default nucleation parameterization used with MOSAIC in the public release of WRF-Chem, and is used in our study for that reason. The Wexler parameterization defines a critical H_2SO_4 concentration at which the nucleation rate is approximately 1 particle cm^{-3} s^{-1}, based on early classical BHN results. When the ambient gaseous H_2SO_4 concentration exceeds this critical concentration, all gaseous H_2SO_4 in excess of the critical value is used to produce new particles having a diameter equal to the smallest diameter covered by the model's sectional framework (e.g., 1 nm in the 20 size bin framework or 39 nm in the 8 size bin framework).

In the Vehkamaki parameterization, theoretical BHN nucleation rates (derived by Vehkamaki et al., 2002) over a wide range of temperature, relative humidity, and gaseous

H_2SO_4 concentration are approximated (fitted) by a rather complicated analytical expression involving exponentials and polynomials of order 1 to 3.

We performed simulations using the Wexler and Vehkamaki parameterizations with the 20 size bin sectional framework, and using the MOSAIC WRF-Chem default configuration of the Wexler parameterization with the 8 size bin sectional framework. Due their poor performance, the results from the 20 size bin Wexler and Vehkamaki simulations are not presented; these simulations were not able to reproduce either the observed new particle formation events or the observed particle number concentrations. In addition, Zhang et al. (2010b) note that the Wexler parameterization often produces unrealistically high nucleation rates. We performed simulations with three of the recent empirical nucleation parameterizations using the 20 size bin sectional framework. These parameterizations are used in the boundary layer, while following Matsui et al. (2011) the Wexler parameterization is applied in the free troposphere. For the activation type nucleation (ACT) and kinetic type nucleation (KIN), the formation rates of 1 nm particles are linear or second-order functions of H_2SO_4 concentration defined as:

$$J=k_{ACT}\times[H_2SO_4], \quad (1)$$

and

$$J=k_{KIN}\times [H_2SO_4]^2, \quad (2)$$

Previous studies showed that k_{ACT} and k_{KIN} coefficients derived from observations in different locations span several order of magnitude: k_{ACT} ranges from 3.3×10^{-8} s^{-1} to 3.5×10^{-4} s^{-1} (i.e. Sihto et al., 2006, Riipinen et al., 2007); while k_{KIN} ranges from 2.4×10^{-15} cm^3 s^{-1} to 1.3×10^{-10} cm^3 s^{-1} (Riipinen et al., 2007; Kuang et al., 2008). In this study we use $k_{ACT}=2\times10^{-6}$ s^{-1} and $k_{KIN}=2\times10^{-12}$ cm^3 s^{-1}, following Reddington et al. (2011). Cui et al. (2014) also recommend the use of $k_{ACT} = 2x10^{-6}$ s^{-1} based on the measured formation rates of ultrafine particles over a pine forest.

Although the ACT and KIN parameterizations have been used in many studies (i.e. Spracklen et al., 2006, Kuang et al., 2008, Mertzger et al., (2010) showed that organic vapors are important for the nucleation processes. We therefore performed an additional simulation using the combined organic and H_2SO_4 mechanism (ORG):

$$J=k_{ORG} \times [H_2SO_4] \times [NucOrg], \quad (3)$$

where k_{ORG} = 5×10^{-13} cm^{-3} s^{-1} as in Reddington et al. (2011) and NucOrg are low-volatility organic vapors that are involved in the new particle formation process.

Previous studies have defined NucOrg in different ways, and there is considerable uncertainty involving these low-volatility organic vapors. Metzger et al., (2010) assumed that the organic vapors involved in nucleation were the same as those involved in the initial condensational growth of the nuclei, and they derived NucOrg concentrations from laboratory experimental data and the initial growth rates. Redington et al., (2011) assumed that the organic vapors involved in NPF were the first stage oxidation (with O_3, OH, NO_3) products of monoterpenes (with a 13% molar yield) and treated them as non-volatile, The studies made Riipinen et al., (2011), Yli-Juuti et al., (2011) assumed that the organic vapors have very low vapor pressures. Using the TOMAS model, Pierce et al., (2011) performed several sensitivity studies to analyze the impact of organic vapors saturation pressure on the growth of nanometer particles and showed that ultrafine mode particle composition is dominated by low-volatility SOA species (those with C* less than 0.001-0.01 μg m^{-3}). Recently, Schobesberger et al., (2013), Ehn et al., (2014), Jokinen et al., (2015) used extremely low volatility organic compounds (ELVOC) formed as first stage oxidation products of monoterpene with different yields (1-17 %) to account for the role of organic vapors in the early stage of new particle formation.

In our model treatment, NucOrg consists of the organic vapors with the lowest C* of the VBS approach. This includes the C* = 0.001 μg/m^3 species from the non-traditional SOA precursors (semi-volatile and intermediate-volatility organics associated with fossil and biofuel combustion and biomass burning) and the C* = 0.1 μg/m^3 species from the traditional SOA precursors (isoprene, terpenes and aromatics) included in this study. Following Yli-Juuti et al. (2013), an upper limit of 10^8 molecules cm^{-3} for the NucOrg is used in Eq. (3). In our simulations, we find that during initial particle formation periods, 96-99% of the growth involves the C* = 0.001 μg/m^3 organic vapors, while the C* = 0.1 μg/m^3 species contribute on average ~7 times more to the ORG nucleation rate compared to those species having C* = 0.001 μg/m^3. The volatilities of some of these species may in fact be too high to actually participate in nucleation, in which case they can be viewed

as proxies for the even lower volatility species that do participate.

Once formed, the new particles then grow by condensation of inorganic and organic gases, and for the small initial sizes, the Kelvin effect influences the condensation rates. MOSAIC treats the Kelvin effect for the condensation of inorganic gases (although H_2SO_4 is treated as non-volatile), but the SOA gas-particle partitioning treatment was modified to include the Kelvin effect. We assume a surface tension of 50 dyne cm^{-1}, and a molecular weight of 250.0 g mol^{-1} for the NucOrg organic vapors, so at 298 K, the Kelvin effect increases the effective saturation vapor concentrations over 1 nm particles by a factor of 55.

Budget diagnostics for aerosol nucleation, emission, condensational growth, coagulation, transport, dry deposition and total tendencies (the sum of all the individually computed tendencies) were saved to illustrate when and where new particle formation events occurred and better understand how they influence the evolution of the aerosol size distribution.

We also performed two additional simulations with the ACT parameterization. One used 12 discrete size bins, also ranging from 1 nm to 10 μm diameter, with good resolution in the size range of interest to this study (new particle formation). The other used the MOSAIC default 8 size bins, with diameters ranging from 40 nm to 10 μm, to quantify the performance and computational cost of this size bin structure compared to the 12-bin and 20-bin versions. In order to account for coagulation losses during nuclei condensational growth from 1 nm to 40 nm in the 8 bin version, we applied the Kerminen and Kulmala (2002) parameterization (KK2002 hereafter). The coagulation loss depends on the growth time from the initial nuclei size to a larger size, and KK2002 estimates this growth time by assuming that the growth is due to H_2SO_4 condensation only. This was modified as follows to also account for condensation of organic vapors. In the 20 bin simulations at individual grid points and times, the growth time from 1 to 40 nm due to H_2SO_4 condensation only and due to H_2SO_4 plus organics condensation were estimated using the condensed masses from the MOSAIC aerosol chemistry module, and the ratio of these two growth times gave an organics enhancement factor for 1 to 40 nm growth (Y). The same calculations were done for growth from 40 to 63 nm giving another

organics enhancement factor (X), and both X and Y were output. After the simulation, a zero-intercept linear regression of Y vs. X was performed (Y = aX), using the entire X and Y data. In the 8 bin simulations, we calculated an organics enhancement factor for growth from 39 to 78 nm (X'), which is the width of the first bin in this configuration. We then estimated the organics enhancement factor for 1 to 40 nm growth as Y' = aX', and applied this enhancement factor to the H_2SO_4 only condensation growth time used in KK2002.

In addition to improving simulations of the aerosol formation and growth processes in MOSAIC, the results of this study will form the basis of incorporating one or more new nucleation schemes into the public version of WRF-Chem.

4 Results

The discussion of the model results focuses on the NPE observed between June 7 and 16, 2010. The prevailing westerly to southwesterly atmospheric flow on June 7-9 and 15-16 transported SO_2 from the San Francisco Bay area to the vicinity of Sacramento and produced NPE on these days. Due to changes of synoptic conditions associated with a trough formed over the western US from June 10 to June 14, 2010 (Fast et al. 2012), weak or no NPEs were observed at the T0 (urban) and T1 (rural) sites on these days. The shift to strong northerly winds led to a decrease of Bay Area emissions transported over Sacramento, consequently decreasing SO_2 and the total observed particle number concentration. We first evaluate the overall impact of the nucleation parameterizations on particle number and size distribution at the surface and aloft, using measurements collected at the T0 and T1 sites as well as along G-1 aircraft flight paths during the June 7 to 16 period. We then provide a more detailed analysis of the simulated formation of new particles and growth at ground level for an observed NPE on June 8, 2010 and on June 12, 2010 when no NPE was observed. Finally, we determine how the differences in particle number and size distribution associated with the nucleation parameterizations affect predicted CCN.

4.1 Temporal Variability in Particle Number Concentration

The ability of the model to simulate the observations is evaluated using statistical scores including normalized mean bias (NMB), and the correlation factor between simulated and measured values (R). Due to the minimum cutoff size of the SMPS instrument, we investigated the behavior of CN10 (particle number concentration having Dp $\geq$ 10 nm), CN40 (Dp $\geq$ 40 nm) and CN100 (Dp $\geq$ 100 nm). Tables 1 and 2 present NMB and R for these three parameters from four model configurations at the T0 and T1 sites. Model performance in simulating PM_1 and $PM_{2.5}$ concentrations using the default WRF-Chem 8 size-bin and Wexler nucleation parameterization configuration (WEX-8BIN) for the entire CARES domain, including the T0 and T1 sites, has been presented in Fast et al. (2014). In general, simulated PM1 is fairly close to observed during 7 – 16 June 2010 both in terms of mass concentrations (NMB=15% at T0 and NMB=-18% at T1) and temporal evolution (R=0.56 at T0 and R=0.64 at T1). However, the WEX-8BIN simulation does not reproduce as well the CN100 concentration (NMB=-55% at T0 and NMB=-65% at T1) nor the temporal evolution (R=0.32 at both sites).

As shown in Figs. 1 and 2, the overall temporal variability of high particle concentrations before and after the passage of the trough between June 10 and 14 was generally captured by the explicit (20 size bin) nucleation schemes used in our study, although they usually overestimate the observed particle number concentrations.

First, we analyze how the standard configuration of WRF-Chem (8BIN) behaves compared to the measurements. Since the 8BIN simulation does not explicitly resolve nucleation and the geometric diameter range for the smallest size bin is from 39 to 78 nm, only CN40 and CN100 are examined. As can be seen from Figs. 1 and 2, the WEX-8BIN simulation is able to reproduce the observed diurnal and multi-day variation of CN40 (R = 0.31 and 0.57 for the T0 and T1 sites, respectively), and largely underestimates the observed number concentration for both the T0 and T1 sites (see Tables 1 and 2). In the case of CN100, the 8BIN simulation also tends to underestimate the observed concentration (up to 65% at the T1 site) with CN100 R values of 0.60 and 0.32 calculated between observations and modeling results at the T0 and T1 sites, respectively.

We now discuss how well simulations conducted using the empirical nucleation parameterizations with 20 size bins agree with the measurements. All three empirical

nucleation parameterizations reproduce the overall observed daily variability as shown Figs. 1 and 2, although during the NPEs they usually overestimate the PNC in different size ranges. The ACT, KIN and ORG simulations overestimate the observed CN10 (from 178% for ACT up to 255% for KIN), although the correlation coefficient suggests reasonable agreement in temporal variability between observations and modeling results ($R > 0.70$). The overestimation is reduced for the CN40 and CN100 particles, and the best results are obtained at the rural T1 site that is not influenced by as high anthropogenic emission rates (see Table 1, 2). Moreover, during the southwesterly flow periods the maximum peaks of CN10 are overpredicted within a factor of 3 by all explicit mechanisms involved in our simulations, while the CN40 and CN100 maximum peaks tend to be overpredicted by a factor of 2 (Figs, 1, 2). The normalized mean bias of CN10 during this period ranges from 187 % for ACT to 347 % for KIN. The overprediction factors for all three empirical parameterizations are reduced during the northerly flow period, when SO_2 transport through the Carquinez Strait to the measurement sites is significantly reduced. During this period the normalized mean bias of CN10 particles is lower and ranges from 129% for ACT to 278 % for KIN. Based on this analysis of PNC in several size ranges, we conclude that for both measurement sites, the ACT parameterization performs somewhat better than the KIN and ORG parameterizations.

New particle formation depends on the concentrations of low-volatility vapors involved in nucleation and the initial growth of the nucleated particles and the coagulation losses of new particles during their initial growth. The low-volatility vapor concentrations depend on their photochemical production and condensational loss to particles. When evaluating and comparing nucleation schemes, it is useful to compare measurement-based and simulated estimates of these sources and sinks. The concentrations and photochemical production of low-volatility vapors was not measured, but we can compare modeled and observed precursor gas (i.e., SO_2) concentrations. For the entire period, the modeled SO_2 concentrations at T0 were fairly close to observed, with NMBs of 30% , but there was poor agreement in temporal variability ($R=0.30$). The coagulation sinks for 1 nm particles and the condensation sinks for H_2SO_4 and at T0 and T1 were calculated (offline) using observed and simulated size distributions of 10 -700 nm particles. The temporal variability of the coagulation and condensation sinks is fairly well

reproduced (R between 0.67 and 0.76). At T0, the simulated coagulation and condensation sinks were about twice those calculated using observations (NMBs of 94% and 106%), while at T1 the coagulation and condensation sinks had NMBs of 35% and 40%. These biases are generally consistent with the CN100 biases at the two sites. The high biases for the condensation and coagulation sinks would tend to give lower new particle formation under the simulation conditions compared to observed conditions, and thus cannot account for the higher simulated NPF (e.g., CN10) in the simulations compared to observations. Also, differences among the simulations with different nucleation parameterizations for SO_2 concentrations and the two sink terms were small, so biases in them compared to the observed (or observation-based) values should have had similar impacts on NPF in all three simulations.

4.2 Analysis of the observed NPE on June 8, 2010

Figures 3 and 4 compare the hourly modeled and observed number size distributions as a function of particle diameter at the T0 and T1 sites, respectively, on June 8. For this study we have adopted the classification of the observed nucleation events given by Boy et al., (2008). Based on occurrence and clarity of new particle formation events, they define four categories: A-event days, B-event days, undefined, and non-event days. According to their classification an A-event shows a clear nucleation mode particles (the highest number of particles are observed at the lowest measurable SMPS size) and subsequent growth to larger sizes; a B-event is less clearly than an A-event (the highest number of particles are not observed in the first SMPS size bin, but at a greater diameter) and it is followed by the subsequent growth. Non-event days are those with no particle formation, while the days that cannot be classified as event or non-event days are called undefined days. Following this classification, on June 8, 2010 for both the T0 and T1 sites a "class B" event occurred. Thus, the highest concentration of particles are not observed in the first SMPS size bin (~12.2 and 8.75 nm diameter at the T0 and T1 sites), but at a greater diameter (~13.6 and 16 nm diameter at the T0 and T1 sites on this day), and growth of these particles to Aitken mode was observed (Figs. 3a, 4a).

All of the simulations captured the observed NPE but with different PNC. The ACT, KIN, and ORG schemes behave similarly on this day, leading to a daily NMB for CN10 of 234%, 346%, and 206% at the T0 site and 143%, 198% and 175% at the T1 site, respectively. Correlation coefficients were between 0.89 and 0.92, indicating a good temporal agreement between observed and simulated CN10.

Observations at both sites show an increase of particles in 10-20 nm range around 0900 PST (Figs. 3a, 4a). These particles continue to grow in size in the following hours until they reach 80-100 nm. Although the observed onset of nucleation starts around 0900 PST, in our simulations the onset of nucleation is two hours earlier (Figs. 3b,c,d; 4b,c,d). This behavior could be attributed to the break-up of stable nocturnal boundary layer and vertical mixing with cleaner air from the lower troposphere, which can trigger the formation of new particles (Kristensson et al., 2008). On this day, the simulated boundary layer growth at the T0 site was very similar to that derived from radiosonde observations; therefore, vertical mixing associated with the growing convective boundary layer is likely reasonably simulated by the model. From the comparison of simulated CN10 aloft with the measurements during the morning G-1 flight on this day, the overestimation factors for CN10 aloft (90%, 73%, and 118% for ACT, KIN, and ORG are much lower than for the surface sites. Therefore, the cleaner simulated free troposphere air could enhance formation of new particles near the surface as the boundary layer grows, as shown in Fig. 5. This figure also shows that for ACT the highest concentration of small particles coming from the nucleation process occurs at ~2/3 of the boundary layer height. A higher number of small particles exist at this altitude compared to the number predicted at the surface, with concentrations aloft ~30% and ~25% greater at T0 and T1, respectively. These particles formed aloft would be quickly transported to the surface by turbulent vertical mixing. KIN acts in a similar manner as ACT, although it predicts an increased number of small particles. In contrast, ORG predicts that the highest concentration of particles occurs at the surface. We can associate this with the relatively high NucOrg concentration predicted at the surface compared to the upper layers; therefore, enhanced particle production at this level is not unexpected when the ORG parameterization is used. In addition, the simulated growth of particles corresponds to the increase of fine-particle SOA mass (Fig. 6), which also starts about 2 h

before the observed NPE, indicating that SOA might have contributed to the simulated growth of ultrafine particles.

We calculated the observed and modeled growth rate of 10-40 nm particles as follows. Following Jeong et al. (2010), the geometric mean diameters (GMD) of 10-40 nm particles were calculated from the size distributions during the period when growth after formation was observed/modeled. The growth rate was obtained by fitting the GMD trend during the growth period:

$$GR = \frac{\Delta GMD}{\Delta t} \quad (4)$$

Thus, we obtained at T0 a GR_{OBS}=2.57 nm h^{-1}, GR_{ACT}=1.43 nm h^{-1}, GR_{KIN}=1.14 nm h^{-1}, GR_{ORG}=1.71 nm h^{-1}, and at T1 a GR_{OBS}=3.69 nm h^{-1}, and GR_{ACT}=1.78 nm h^{-1}, GR_{KIN}=1.51 nm h^{-1}, GR_{ORG}=1.92 nm h^{-1}. This indicates that the simulated growth rate was always slower than observed, which could be due to an underprediction in the concentration of condensable vapors compared to those in the ambient air or to the current treatment of SOA that does not include changes to viscosity and/or effective volatility by particle-phase aging processes (Shrivastava et al., 2013; Zaveri et al., 2014).

The observed continuous growth of nucleation mode particles through the day at both T0 and T1 sites (Figs, 3a, 4a) suggests that nucleation and growth take places over regional scales. Figure 7a shows the simulated nucleation rate (from ACT) averaged from the surface to ~130 m above ground level from 0500 PST to 0900 PST on June 8, 2010. Superimposed on this figure is a back trajectory (at 100 m AGL) for air arriving at the T0 site at 0900 PST on this day. The back trajectory indicates the air mass is transported by southwesterly winds from the San Francisco Bay area through the Carquinez Strait into the Central Valley before arriving in Sacramento. The peak nucleation rates occur over industrialized region along northern San Francisco Bay that extends towards the T0 site. Nucleation also occurs over most of the Sacramento Valley, but the rates are about an order of magnitude lower than between the Carquienez Strait and Sacramento. Fig. 7b shows the computed PNC in the 1-10 nm (CN_{1-10}), 10-40 nm (CN_{10-40}) and 40-100 nm (CN_{40-100}) ranges along the trajectory. High concentrations of CN_{1-10} and CN_{10-40} particles occur along the trajectory prior to their arrival over the T0 site. The sharp increase of CN_{1-10} particles after 0500 PST June 8, followed two hours later by the increase of CN_{10-}

$_{40}$ particles are associated with the early morning onset of nucleation. The model results indicate that nucleation and growth of aerosol particles were not only a local phenomenon, but also took place upwind of Sacramento before being transported over the T0 site (see Fig. 7a,b).

To obtain a better understanding of the factors that contribute to differences in the simulated number size distribution among the different parameterizations, we use budget diagnostics. These diagnostics are the tendencies associated with dry deposition plus vertical turbulent mixing, other transport (advection and horizontal turbulent mixing), emissions, condensation, nucleation, coagulation, and total tendency that affect PNC in the 1-10, 10-40, and 40-100 nm diameter ranges. (Note that the coagulation tendencies for each size range are combined losses from self-coagulation and coagulation with larger size particles.) As shown in Figs. 8, 9, and 10 the use of different nucleation parameterizations leads to differences associated with the processes that contribute to aerosol formation and growth.

Even though both the ACT and KIN parameterizations depend only on H_2SO_4 concentration, the differences in their formulation lead to differences in the nucleation rates and consequently CN10 concentration, as shown previously. The KIN nucleation rates are higher than the ACT nucleation rates by as much as 1474 % and 930 % at the T0 and T1 sites, respectively. These differences in the nucleation rate could explain the differences in the magnitude of the budget terms associated with condensation (Figs. 8c, 9c, 10c), coagulation (Figs. 8e, 9e, 10e) and predicted particle number concentration in the 1 to 10 nm range (Figs. 8g, 9g, 10g). Moreover, these differences in the nucleation rate could also explain the magnitude of combined nucleation and coagulation processes (Fig. 8h) that suggest for ACT the coagulation loss is more important than nucleation production. Similarly, the higher predicted nucleation rate for KIN (Fig. 8d) could explain the difference in predicted number concentration in 1 to 10 nm range (Fig. 8g). The aforementioned budget terms (nucleation, condensation, and coagulation) that contribute to the formation and growth of particles are strongly correlated with the diurnal variation of H_2SO_4 concentration at both sites on this day (less so with the ORG parameterization), although their magnitudes highly differ. Note that the diurnal variations of budget terms for dry deposition plus vertical mixing and for other transport

for 10-40 and 40-100 nm particles are similar among the ACT, KIN, and ORG simulations (Figs. 9a, b; 10a, b), but the diurnal variations in these budget terms for 1-10 nm particles are quite different among the three nucleation parameterizations. Fig. 8a shows that while the CN1-10 in KIN are lost through deposition and vertical mixing processes, a net gain of particles is predicted during mid-day hours and late afternoon using ACT, showing the impact of vertical mixing on predicted number concentration at the surface. Moreover, analysis of the other transport budget term (Fig. 8b) shows an increase of CN1-10 at T0 starting with the onset of modeled nucleation for both the ACT and KIN parameterizations, but a weak decrease for the ORG parameterization. These findings confirm that the nucleation and growth of aerosol particles are not just a local phenomenon but take place over a regional scale. A net gain of particles transported from upwind is simulated using ACT in the late afternoon (Fig. 8b), suggesting that the differences associated with the nucleation parameterization formulation and their strength impacts non-local phenomena such as horizontal transport.

We note that the use of the ACT and ORG schemes leads to similar results in terms of total PNC and size distribution during this day, whereas the budget diagnostic terms show several differences. Pierce et al., (2012) found a relatively small difference between ACT and ORG scheme simulations, which they attributed to high correlations of both H_2SO_4 and low-volatility organics with sunlight. In our simulation only H_2SO_4 is highly correlated with downward short wave flux (R = 0.83 over 0600 to 2000 PST), while the low-volatility NucOrg concentrations are relatively poorly correlated with the downward shortwave radiation flux (R = 0.38). As shown in Fig. 11, the daily variability of H_2SO_4 and NucOrg concentrations present a different behavior, with H_2SO_4 concentrations peaking at 1.34e8 molecules cm^{-3} close to 1300 PST and NucOrg concentrations peaking at 6.57e6 molecules cm^{-3} around 1700 PST. Using Mikkonen et al. (2011) method, we calculated the H_2SO_4 proxy concentration on June 8 using observed SO_2 and particle concentrations. The average daytime concentration of this H_2SO_4 proxy is a factor of ~3 higher than the modeled H_2SO_4, but the proxy and modeled H_2SO_4 concentrations have similar temporal variations, peaking near noon PST . Although both H_2SO_4 and NucOrg are formed by oxidation of precursor gases by OH radicals, and hence are linked to solar radiation that regulates the intensity of photochemical reactions, their different diurnal

patterns can be related to the diurnal patterns of their respective precursor gases. The anthropogenic organic vapor with the C* = 0.1 μg/m^3 has the highest contribution to the NucOrg vapors concentration at T0, and their concentrations start to increase at 1300 PST and reach a maximum around 1800 PST. Their aromatic precursor gas has a similar temporal pattern during the afternoon, while SO_2 is decreasing during this period (not shown).

The nucleation budget term demonstrates the impact of these low-volatility gases on the new particle formation. The ORG budget terms and particle number concentration for 1-10 nm particles have a different diurnal variability compared to ACT (Fig. 8). As can be seen from Figs. 8d and 8g, the ORG scheme shows two peaks in particle concentration that are associated with the increase of H_2SO_4 concentration in the morning, and the increase of low-volatility NucOrg concentration during the afternoon. As in case of ACT and KIN, the ORG budget terms associated with condensation (Figs. 8c, 9c, 10c), nucleation (Fig. 8d) and coagulation (Figs. 8e, 9e, 10e) show the connection of these terms to the way that the nucleation is parameterized. Still, the budget terms and predicted number concentration (Figs. 9g, 10g) in the 10-40 nm and 40-100 nm size range present almost the same daily variability for all aforementioned parameterizations. Thus, we can say that even though the treatment of NPF has a great impact on the production rate of freshly nucleated aerosols (Fig. 8), removal processes through condensation, coagulation or dry deposition are efficient and could explain the relatively similar CN40 and CN100 predicted by ACT, KIN and ORG schemes. This is in agreement with the Westervelt et al. (2014) study with the GEOS-Chem-TOMAS modeling system, which showed that CN10 concentrations are more sensitive to BL NPF parameterizations than CCN-sized particle concentrations, consistent with the loss of newly formed particles through coagulation. Moreover, they investigated the nucleation rate and gas condensation sinks impact growth rate, coagulation sink, and survival probability, and showed that the relatively small differences in the predicted BL CCNs concentration are due to a strong damping effect. This might also explain the relative insensitivity of CN40 and CN100 to choice of NPF mechanism in our study. Analyzing the total tendency of particle number we note that particles in 1-10 nm range have a net gain of particles starting around 0500 PST (Fig. 8f); this trend is kept for larger particles,

with a modeled net gain that starts around 0600 PST for particles in 10-40 nm range (Fig. 9f) and around 0800 PST for particles in 40-100 nm range (Fig. 10f). This behavior is in accord with new particle formation and growth processes.

In general, the simulations also capture the observed simultaneous decrease of particle size and number concentrations during the afternoon, as can be seen in Figs. 1 and 2. The size distribution changes are more clearly seen in Fig. 12, which shows the observed and simulated particle number distributions at 0600, 1400, and 1900 PST on June 8, 2010. The measurements show that the 20-100 nm PNC increases between 0600 and 1400 PST, presumably due to nucleation and condensational growth. Particle concentrations decrease later in the afternoon as nucleation rates decrease and the wind direction shifts. All nucleation schemes reproduced this variation in 20-100 nm PNC during the day at the T0 site, while at the T1 site both the observed and simulated PNC did not decrease between 14 and 19 LST. Southwesterly winds during the afternoon of June 8 transported air from the vicinity of Sacramento to the T1 site and kept concentrations of small particles relatively high.

In summary, we show that all the empirical parameterizations used in our simulations were able to qualitatively reproduce characteristics of the observed NPE on June 8, 2010. However, for all parameterizations the onset of the NPE was about 2 h too soon and the simulated PNC was too high. From the analysis of budget diagnostic terms for 1-10 nm particles, we find that at both T0 and T1 sites on this day, the ACT and KIN simulations exhibit almost the same temporal variability and are highly correlated with the diurnal variation of H_2SO_4 concentration. In contrast to the ACT and KIN simulations that show one peak in nucleation rate around noon, the diurnal variability from the ORG simulation is different, showing two peaks for nucleation rates and many other differences in budget diagnostic terms for 1-10 nm particles. Thus, the different nucleation parameterizations lead to different results in both particle number and size distribution.

4.3 Analysis of an observed non-NPE on June 12, 2010

On June 12, 2010, modest increases in CN10 were observed at the T0 and T1 sites during the day (Figs. 1 and 2). The observed size distributions in Figures 13a and 14a show that

the number of particles in 10-30 nm size range increased during the day, but this was not followed by particle growth to larger sizes, as was the case on June 8, 2010. Although some nucleation was likely occurring, this behavior does not qualify as a nucleation event, based on the Boy et al., (2008) classification. The daily NMB values show that ACT, KIN, and ORG simulations overestimate CN10 by 192%, 199%, and 307%, respectively, at the T0 site and by 139%, 313% and 118%, respectively, at the T1 site. Correlation coefficients between observed and simulated values range between 0.40 and 0.49, indicating that these parameterizations coupled with other model processes did not capture the observed diurnal variability as well as on June 8.

The observed particle number size distribution at the T0 site shows a shift in the maximum from 10-30 nm range to 20-50 nm range after 1900 PST (Fig. 13a). All simulations reproduce this feature, although the shift in size is between 20 and 80 nm and the PNC is too high.

A possible explanation for this observed and also modeled feature can be related to the structure of the boundary layer. In contrast to the growth of the convective boundary layer during the day, the simulated boundary layer collapses after 1800 PST, coinciding with increased stability near the surface. This stability does not allow vertical mixing of air near the surface with air aloft, so large particles remain near the surface, and this leads to the simulated increase in the 20-80 nm range. Again, as in the case of June 8, we speculate that the change in wind direction and the decrease of wind speed between 1800 and 1900 PST might also explain the shift in particle size distribution. With lower wind speeds, we have a reduced effect of horizontal transport and vertical mixing on the 1-10 and 10-40 nm range particles (Figs. 15b, 16b). At the same time we noticed a net gain of particles in the 40-100 nm size range (Fig. 17c), most likely coming from the condensation of NucOrg species, that is within an order of magnitude higher than the predicted H_2SO_4 (Fig. 11).

As in case of June 8, 2010, the analysis of budget terms associated with the formation and growth of particles together with the predicted number concentration shows that the differences in the nucleation rate formulation lead to relatively large daily variability in the 1-10 nm size range (Fig. 15), while these differences are generally much smaller in

the 10-40 nm and 40-100 nm size ranges (Figs. 16, 17). For this particular case, most budget terms for ACT and KIN are similar for all size ranges (Figs. 15-17), although nucleation and coagulation for 1-10 nm particles is larger for KIN, while ORG shows the impact of low-volatility NucOrg organic vapors on the nucleation rate and subsequent influence on diurnal variation. During this period, the amount of SO_2 transport to the site is small, so there is less H_2SO_4 present compared to the low-volatility NucOrg generated from local sources. Thus nucleation and subsequent growth of new particles is greater in case of the ORG simulation because of the local sources of NucOrg species, leading to the larger overestimation of 1-10 nm (Fig. 15g) and 10-40 nm particles (Fig. 16g) at the T0 site compared to the other mechanisms.

Due to missing measurements between 1200 and 1800 PST, the evolving observed particle number size distribution at the T1 site (Fig. 14a) is not complete. Still, as for the T0 site, we can observe at T1 a maximum in size distribution at 1100 PST in the 10-30 nm range which is shifted towards the 30-50 nm range after 1800 PST. However, the simulations are not able to reproduce this feature, with the model indicating a shift from the 6-10 nm to the 10-20 nm range. From an analysis of the budget terms and the NucOrg gas concentration, we can attribute the shift in the T1 size distribution around sunset to the same causes as the T0 shift, namely the boundary layer collapse, variations in wind speed and direction, and (for the ORG parameterization) the condensation of NucOrg organic vapors.

4.4 Impact of nucleation parameterizations on physical processes associated to the NPEs

Table 3 shows selected budget terms on all NPE days (June 7-11 and June 14-16, 2010 at the T0 site, and June 7-10 and June 14-16 at the T1 site) averaged over the period from 0400 PST through 1600 PST. These terms show how the particle number concentrations are affected by the different processes. The four terms for CN1-10 particles comprise a complete budget: gain due to nucleation, loss due to coagulation, loss due to condensational growth to sizes > 10 nm, and net transport plus deposition (advection, vertical mixing, and dry deposition). The single term for CN10-100 particles shows the net gain by condensational growth of smaller particles into this size range, modulated by

coagulation loss of CN10-100 particles (which is significant on some days). On each NPE day, the nucleation budget terms for 1-10 nm particles from the three nucleation parameterizations differ by factors of about 10 to 50. The ACT nucleation term is always the smallest, and there are large differences between KIN and ORG on many days, with KIN largest on some days and ORG largest on others. Yet, the nucleation and coagulation terms are similar in magnitudes for any given parameterization and day, indicating that coagulation strongly moderates the large differences in nucleation rates. This sustains the findings from the diurnal variability analysis of June 8, 2010 NPE.

The CN1-10 condensation budget terms for all three parameterizations are much closer in magnitude to each other, generally within a factor of 2, except for the June 7, 2010 case when the condensation budget terms are higher by factors of 4.6 and 5.6 for KIN and ORG compared to ACT. The CN1-10 condensation budget term (when multiplied by -1) gives the effective production of particles larger than 10 nm diameter. These effective CN>10 production rates are thus much less sensitive to the nucleation parameterizations, and are also much smaller in magnitude than the nucleation rates, because of the strong modulation of nucleation by coagulation.

The combined condensation and coagulation budget terms for 10-100 nm particles are quite similar to the CN1-10 condensation on some days but are lower by factors of about 2 to 4 on other days, indicating further modulation of the new particle production by coagulation on some days. For the June 7, 2010 case noted above, the combined CN10-100 condensation and coagulation terms from the three nucleation parameterizations are somewhat closer (factor of 2.8 range) compared to the CN1-10 condensation (factor of 5.6 range) due to this additional modulation. Note that the CN10-100 condensation plus coagulation term for KIN is on average about 40% higher than for ACT, and this is in agreement with the KIN vs. ACT CN10 concentration differences presented in section 4.1.

The differences in the CN1-10 budget terms for horizontal transport, vertical mixing and dry deposition indicate the impact of nucleation and growth processes over regional spatial scales. As stated previously, the efficiency of removal processes such as condensation, coagulation or dry deposition could explain the relatively small differences

among simulations for the predicted particle number concentrations in the 10-40 nm and 40-100 nm size ranges (see Figures 1 and 2 and Table 3). Once more, we have shown that although the formulation of the nucleation rate parameterization impacts the prediction of newly formed particles, removal processes strongly modulate the nucleation parameterization differences.

4.5 Comparison with aircraft measurements in the and above boundary layer

As shown in Table 4, all simulations produced average particle number concentrations aloft that were generally too high when compared to the CPC measurements collected during the eight aircraft flights. The statistics for particles with diameters greater than 3 nm (CN3) show that all parameterizations predicted more particles in the nucleation mode than were measured. The best results were obtained from the ACT simulation (NMB ranging from 157% to 274%) and the worst results were obtained for the KIN simulation (NMB ranging from 162% to 845%). A similar statistical trend occurred for CN10, except that the differences between model results and observations were greatly reduced compared to CN3. For CN10, the KIN simulation had a NMB between 105% and 338%, while the ACT simulation had a NMB between 69% and 230%.

There are a few instances, such as the flight during the afternoon on June 8 (flight 08b), in which the statistical analysis shows that all the simulations reproduced the observed spatial variability of CN3 and CN10 reasonably well ($R > 0.67$ and $R > 0.77$), while overestimating the observed concentration (CN3 concentration has a NMB ranging from 204% for ORG to 603% for KIN while CN10 concentration has a NMB ranging from 162% for ACT to 219% for KIN). There are other cases for which the simulated CN3 and CN10 concentration have similar high biases, but the simulated spatial variabilities do not agree well with the measurements (low correlation), such as on the afternoon of June 12, 2010 (flight 12b).

To summarize the overall performance of the different simulations we also computed statistics for all flights combined (see Table 4). As for individual flights, the best results were obtained when using the ACT parameterization (NMB of 226% and 162% for CN3

and CN10, respectively) and the worst results were obtained for the KIN parameterization (NMB of 608% and 239% for CN3 and CN10, respectively). The correlation coefficients (between 0.48 and 0.54) show a moderate agreement in capturing the observed spatial variability of both CN3 and CN10.

We also examined the model performance in simulating CN3 and CN10 as function of aircraft altitude, using intervals from the ground to 500 m, 500 to 1000 m, 1000 to 1500 m, and 1500 to 2000 m agl. Comparisons between the measured and predicted median PNC, together with 25^{th} and 75^{th} percentiles, for the afternoon flights of June 8 and June 12 are shown in Figs. 18 and 19, respectively. Below 1000 m agl, the simulated CN3 and CN10 concentrations are usually 100-200% higher than the corresponding measurements (see Figs. 18, 19). Note that the afternoon maximum boundary layer height on June 8 was ~800 m agl (Fig. 3), suggesting that the majority of the measured and simulated CN3 and CN10 particles were located within the boundary layer. Comparison between modeled and observed CN3 and CN10 medians and interquartile ranges above 1000 m agl on June 8, 2010 (Fig. 18c,d,g,h) shows that all simulations reasonably represent the measurements. CN3 concentrations have a NMB ranging from 56% for ACT to 211% for KIN, while CN10 is overestimated by 70-100%. This behavior can be associated with lower SO_2 concentrations at these altitudes (simulated but not measured), and consequently lower H_2SO_4 concentrations and less new particle formation.

The strong northerly winds present on June 12, 2010 led to much lower SO_2 concentrations compared to June 8, and this might explain the relatively homogeneous observed and simulated particle number concentrations at different altitudes (Fig. 19). Yet, the median values of CN3 show that our simulations still overestimate number concentrations by up to a factor of 6, especially for KIN and ORG, while the overestimation factor reaches 4.5 for CN10.

This comparison of simulated particle concentrations with the aircraft measurements shows that the three nucleation parameterizations were able to reproduce the temporal and spatial variations in particle number for several flights; however, the simulated concentrations in the boundary layer are too high, especially for the smallest particles.

4.6 Impact of nucleation schemes on CCN concentration

CCN concentration depends on both the particle size distribution and chemical composition. Observational studies have linked nucleation events to CCN production (e.g. Asmi et al., 2011, Wiedensohler et al., 2009). New particles can grow to the size of CCN through condensation and coagulation processes, although only a portion of these particles reach that size. As discussed in Kerminen et al., (2012) and references therein, the connection between the formation of new particles and CCN concentration has recently started to be investigated by using models. They note a non-linear dependence between atmospheric CCN production and the nucleation process due to (1) the nucleation rate, (2) subsequent growth of nucleated particles to larger sizes, and (3) the presence of primary aerosol particles, and pointed out the challenge in accurately predicting CCN concentrations given these factors.

Several studies (e,g. Merikanto et al., 2009, Sihto et al., 2011, Westervelt et al., 2014) have shown that boundary layer nucleation plays an important role in determining CCN number concentration. Kuang et al., (2009) quantified the role of self-coagulation loss (up to 20%), coagulation (up to 10%), condensation on pre-existing aerosols (up to 30%), and condensation on nucleated particles (up to 80%) to the CN100 particles concentration using field study data acquired at three North American locations for twenty CCN formation events. They showed an enhancement on average by a factor of 3.8 of the pre-existing CCN number due to NPF. Using the GEOS-Chem-TOMAS model, Westervelt et al., (2014) calculated particle growth rates, condensation sinks, coagulation sinks, survival probabilities, and CCN formation rates for eight different nucleation parameterization. Their study showed that increases in the nucleation rate led to decreased survival probability, so that the CCN number concentrations are relatively insensitive to the nucleation mechanism. During CARES, CCN number concentrations were measured at both the T0 and T1 sites for several supersaturations (SS= 0.1%, 0.2%, 0.35%, 0.5%). To assess the impact of the nucleation parameterizations on CCN, we next compare observed CCN with simulated CCN number concentration calculated offline using the simulated chemical composition and the hygroscopicity of particles together with their size-dependent number concentration predicted by WRF-Chem. As shown in Tables 5 and 6, the calculated CCN number concentrations generally are weakly

correlated with the measurements. The calculated CCN are generally lower than the measurements, except at 0.5% supersaturation. The underestimation at 0.1% and 0.2% supersaturations is likely to be closely linked to the large number of ultrafine particles that are not activated at these supersaturations, since the effective diameter of CCN is inversely correlated to the supersaturation (Yue et al., 2011). Using the simulated size-dependent particle composition, we calculated particle sizes having critical supersaturations corresponding to the CCN measurement supersaturations. For supersaturations of 0.5%, 0.35%, 0.2%, and 0.1%, the diameters are 56, 78, 125, and 168 nm, respectively, with corresponding average hygroscopicities of 0.24, 0.23, 0.22, and 0.20. There is no clear distinction in these diameters between the T0 and T1 sites. The simulated CCN concentrations at 0.2% and 0.1% supersaturation thus correspond roughly to CN125 and CN168 concentrations. The simulated CN168 particle concentrations are biased high at T0 but low at T1 (NMBs of about 44% and -16%, respectively), which can explain the underestimations of 0.1% SS CCN at T1 but not at T0. The simulated CN125 have high biases at both T0 and T1 (NMBs of about 72% and 21%, respectively), so the cause of the simulations' underestimations of 0.2% SS CCN is not clear. Mei et al. (2013) performed size-resolved CCN measurements of 100-170 nm diameter particles at the T1 site, and they found that 90% or more of the size-selected particles were CCN active and had hygroscopicities between 0.10 and 0.21 (mean of 0.15). This suggests that the simulated low biases for 0.2% supersaturation CCN are not due to differences in simulated vs. observed mixing state and/or hygroscopicity.

Figures 20 and 21 present the times series of observed and calculated CCN at both the T0 and T1 sites for five supersaturations. Comparing observed CCN and CN10 concentrations shows that several hours after the NPEs take place, an increase in CCN concentration is also observed. This is consistent with observational studies around the world that reported a clear increase in the CCN concentration after the occurrence of nucleation events (e.g., Kuwata et al., 2008, Levin et al., 2012). During the northerly wind period, the simulated CCN concentrations better match the observations at the T1 site compared to results at the T0 site. This is likely due to lower PNC biases for all size ranges at the T1 site during the same period, thus also demonstrating the connection between PNC and CCN.

We next analyze how selection of the nucleation parameterization affects the predicted CCN number concentration for one supersaturation (SS=0.5%). For this purpose we compare the ACT, KIN, and ORG results with a simulation in which nucleation (and NPF) was turned off. Compared to the simulation with no NPF, CCN levels at SS=0.5% from ACT, KIN, and ORG are around 18% higher at the T0 site and 26% higher at the T1 site. These changes indicate that nucleation and subsequent growth moderately influences the CCN at this supersaturation. This result has been found in previous studies that report 5 – 70 % of the CCN could be attributed to nucleation (e.g. Spracklen et al., 2010, Pierce and Adams, 2009, Matsui et al., 2013).

For SS=0.5%, the average activation ratios (AR), defined as AR = CCN/CN10, are around 0.10 at both measurement sites for all parameterizations. As pointed out by Andreae and Rosenfeld (2008), low AR are observed with fresh aerosols, whereas AR approaches 1 for aged aerosols. The relatively small ARs obtained for the ACT, KIN, and ORG parameterizations exhibit the importance of freshly formed secondary aerosols and are relatively close to the observed AR (0.14 and 0.21 for the T0 and T1 sites, respectively).

Thus, from the statistical analysis and the temporal evolution of CCN at different supersaturations, we can conclude that nucleation affects both CCN concentrations and the fraction of particles that are available to act as CCN. However, the ACT, KIN, and ORG parameterizations give fairly similar results, especially for low supersaturations, suggesting that CCN at these supersaturations (and sizes) are less sensitive to the nucleation mechanism and rate, possibly due to a slow growth rate of freshly nucleated particles to these sizes and low survival probability (Westervelt et al., 2014), or that the concentrations of these are mainly driven by other processes (e.g., primary aerosol emissions).

4.7 Impact of sectional bin number on predicted particle number and mass concentration

Based on the statistics shown in Section 4.1, the ACT parameterization performed somewhat better for both surface measurement sites and for most of the G-1 aircraft

flights. Therefore, we now focus on comparing the impact of sectional size resolution (number of bins and lowest diameter) on predicted particle number and mass concentrations when the ACT parameterization is used. In addition to the 20-size bin simulation presented previously (hereafter referred to ACT-20BIN), we performed two additional simulations. The, ACT-12BIN simulation uses 12 particle size-bins ranging from 1 nm to 10 μm dry diameter. This bin structure still explicitly resolves new particle formation, while reducing computational costs compared to ACT-20BIN by 36%. Simulation ACT-8BIN employs the default 8-particle-size-bins ranging from 39 nm to 10 μm used by MOSAIC in the publicly released version of WRF-Chem. Note that this configuration does not explicitly treat the growth of freshly nucleated particles (which are placed in the first size bin with 39 nm diameter), and the Kerminen and Kulmala (2002) parameterization is applied to estimate the coagulation loss of new particles during their growth from 1 nm to 39 nm. Using ACT-8BIN reduces the computing cost by 45% compared to ACT-20BIN.

The comparison between standard 8 bin configuration that uses the Wexler parameterization (WEX-8BIN) and 8 bin version that uses ACT (ACT-8BIN) shows an improvement in predicted CN40 concentration when ACT is used (Tables 7, 8). For example, at the T0 site the CN40 NMB is reduced from -34% for WEX-8BIN (Table 1) to -8% for ACT-8BIN (Table 7). However, the statistics for CN100 concentration shows a modest variation between simulations, ACT-8BIN has NMBs of -58% and -67% at the T0 and T1 sites, respectively, compared to WEX-8BIN NMBs of -55% and -65%.

In our simulations, the ACT-8BIN configuration (which does not explicitly treat initial growth and loss of new particles) gives higher CN40 concentrations compared to the ACT-12BIN and ACT-20BIN configurations. This result is counter to the Lee et al. (2013) study that used the TOMAS model with lowest bin diameters of 1 (explicit treatment of initial growth and coagulation loss) and 3 and 10 nm (Kerminen and Kulmala (2002) parameterization) with 40, 36, and 30 size bins, respectively., 3, and 10 nm. They found that the CN10 particles were overpredicted when the Kerminen and Kulmala (2002) parameterization was used. Several factors may explain the differences between Lee et al. (2013) and our study: the nucleation parameterizations (binary/ternary vs. activation type mechanism), lower size bin (3/10 nm vs. 40 nm), analysis period

(average over the spring season vs. 10 days in summer), horizontal resolution (4^{O} latitude x 5^{O} longitude vs. 4 km), emissions inventory, distribution of primary aerosol particles, gas-phase photochemistry, and the estimation of growth time from 1 nm to 40 nm.

As can be seen from Tables 7 and 8, the ACT12BIN simulation produces similar results for CN10 particles compared to the ACT-20BIN simulation, while also showing a visible improvement for CN40 and CN100 particles. The reduced overestimation of CN40 particles by more than 40% could at least partially be explained by the differences in the bin boundaries: the simulated CN40 are calculated as particles larger than 39.8 and 46.4 nm for the 20 and 12 bin configurations respectively (i.e., no interpolation is used).. For CN100 particles the lower bin edge is at 100 nm for both ACT-12BIN and ACT-20BIN, so the lower CN100 (and CN40) with ACT-12BIN suggests that transfer of particles to larger sizes during condensational growth is somewhat slower with the coarser size resolution. The correlation coefficients between observed and ACT-12BIN simulated values are similar to the R values between observed and ACT-20BIN.

Applying the same statistics for the particles collected during the G-1 aircraft flights, we note that both ACT-12BIN and ACT-20BIN overestimate CN3 and CN10 particles (Table 9). However, the use of ACT-12BIN tends to decrease the overestimate of ACT-20BIN in predicted CN3 concentration up to 71 % (June 10, morning flight). The statistics for all flights show an improvement in predicted CN3 number for ACT-12BIN, with a NMB of 194% compared to an ACT-20BIN NMB of 226%, while for CN10 for all flights we obtain similar NMB scores (169% and 162% for ACT-12BIN and ACT-20BIN, respectively). This statistical analysis shows that the use of a 12 bin particle size distribution represents a good compromise between computational time and the aerosol physico-chemical processes included in WRF-Chem.

Analyzing the total mass of aerosol species obtained from the simulations in which the number of discrete size bins is varied, we note that differences between the 20 bin and 12 bin versions are very small. Over the entire analyzed period of June 7-16, 2010, the predicted mass concentration of aerosol compounds varies by ±2 % between ACT-12BIN and ACT-20BIN. The differences are larger when we compare ACT-20BIN and ACT-8BIN, with ACT-20BIN leading to 4% more SO_4 mass, 6% more NH_4 mass, 1% more

NO_3 mass and 5% less OA mass over the entire simulation period. These differences are partly related to the primary aerosol emissions in the 8 bin and 20 bin versions. A small fraction of aerosol mass emissions are in the 10 to 40 nm size range, so emissions in the ACT-20BIN simulation are about 1% larger than in ACT-8BIN. Another factor is the increased surface area of submicron aerosol in the ACT-20BIN simulation compared to the ACT-8BIN simulation.

4.8 Sensitivity to the empirical coefficients of the BL nucleation parameterizations

In order to test the sensitivity of the modeled PNC concentration to the empirical coefficients used in the BL nucleation parameterization, we performed additional sensitivity tests for all the ACT, KIN and ORG simulations in which the empirical coefficients were reduced by a one, and two orders of magnitude. Due to the expensive computational cost, we have done this sensitivity test only for June 8, 2012 case. For CN10 concentrations at the T0 site on June 8, ACT, KIN, and ORG had daily average NMB of 234%, 346%, and 206%; tests with the empirical coefficients reduce by a factor of 10 had NMB of 130%, 291%, and 125%; and tests with the empirical coefficients reduce by a factor of 100 had NMB of 28%, 210%, and 46%. For the T1 site, ACT, KIN, and ORG had daily average NMB of 143%, 198% and 175%; tests with the empirical coefficients reduce by a factor of 10 had NMB of 103%, 165%, and 152% and tests with the empirical coefficients reduce by a factor of 100 had NMB of 38%, 135%, and 78%. These sensitivity tests still overestimate the observed CN10 concentration, and also show that at T1 the model is less sensitive to the empirical coefficients than at T0. This suggests that not only the empirical coefficient is responsible for the simulated PNC, but other factors like model processes, uncertainties in emissions concentration and distribution of primary particles can affect the formation of new particles and their growth. For CN40 and CN100 particle concentrations, we find relatively small differences among different sensitivity tests (NMB variation of ~15% or less), that shows a dampened response to BL nucleation. This demonstrates once again, as was shown in section 4.4, the efficacy of removal processes that causes a greatly reduced survival probability for nucleated particles growing to CCN sizes (e.g. Kuang et al., 2009).

5 Summary and conclusions

The WRF-Chem model v.3.5 was used to simulate the particle number concentration (CN) and size distribution during the CARES field campaign, which took place near Sacramento, CA in June 2010. The MOSAIC aerosol model was extended to incorporate nm sizes of freshly nucleated particles and three state-of-the-science empirical nucleation mechanisms, which were used to investigate how different formulations of the nucleation rate impact the temporal and spatial variations of simulated CN and CCN number concentrations.

By comparing simulation results from the three empirical nucleation parameterizations explicitly treating nucleation using a 20-size bin sectional framework with measurements acquired during the CARES campaign, we showed that the parameterizations generally reproduced the overall observed spatial and temporal variability. However, the simulations with the activation (ACT), kinetic (KIN), and organics+H_2SO_4 (ORG) parameterizations overestimated the observed number concentration for particles with diameters > 10 nm (CN10). In terms of the normalized mean bias (NMB), the best results were obtained using the ACT parameterization (NMB of 178% over the entire analyzed period at the CARES T0 site), while the least favorable results were obtained for KIN (NMB of 255% at the T1 site). This overestimation was reduced for larger submicron particles (CN40 and CN100). Measurements on a day with a new particle formation and growth event (NPE) indicated a diurnal cycle consisting of the onset of nucleation in the morning, subsequent particle growth, and particle number decrease during the afternoon. The cycles predicted from the ACT, KIN, and ORG simulations were similar to observed; the simulated onset of nucleation, however, was two hours earlier than observed and coincided with the onset of SOA formation. For a non-NPE day, our simulations reproduced the observed particle number concentration and the observed late afternoon shift in size distribution associated with the collapse of the boundary layer.

Using budget diagnostic terms we were able to establish how the nucleation rate parameterization affects the source/sink of particles, and also to explain some simulated

features. The different nucleation parameterizations led to differences in the daily variability and magnitude of the budget terms associated with condensation, nucleation and coagulation for particles in the 1-10 nm size range (CN1-10). For example, ACT and KIN exhibit almost the same variability at model locations corresponding to the two surface observation sites on a NPE day, yield one peak in CN1-10 particle number concentration around noon local time, and are highly correlated to the diurnal variation of H_2SO_4 concentration. In contrast, ORG exhibits a different diurnal variation, showing two peaks (morning and afternoon) for most of the budget diagnostic terms for particles in 1-10 nm range. Thus, the different nucleation parameterizations lead to different results in both particle number and size distribution. However, these differences are greatly reduced for larger particles. We conclude that the loss processes are efficient and could explain the relatively similar biases of CN40 and CN100 given by the ACT, KIN and ORG parameterizations. Moreover, the budget diagnostic terms help us to understand modeled features such as the late afternoon shift in the observed and simulated size distribution on the non-NPE day.

We also analyzed the impact of the various nucleation parameterizations on CCN concentrations. We found that although the nucleation process could explain a percentage of CCN number concentration (up to 20-30% at 0.5% supersaturation), the choice of nucleation parameterization had no impact on the magnitude of the predicted CCN number concentration.

Using an intermediate number of size bins (12) to represent the particle size distribution and to explicitly capture the new particle formation process, we obtain CN10 results similar to those obtained using 20 size bins, and improvements (relative to observations) for CN40 and CN100. Thus we can state that the use of a 12-size bin sectional framework represents a good compromise between computational time and the physico-chemical processes included in the WRF-Chem model. Simulations using the MOSAIC default 8-size bin (39 nm to 10 mm diameter) sectional framework and either the ACT or the default Wexler nucleation parameterization underestimate the observed CN40 and CN100 concentrations and do not reproduce the observed daily variability as well as the 20 bin simulations.

We also analyzed the impact of size distribution on predicted aerosol mass concentration. We noticed that between 12 bin and 20 bin frameworks there is little variation over the entire analyzed period. Larger differences are found when we compare 8 bin and 20 bin frameworks, with up to 6% more mass (in the case of NH_4) predicted by the 20 bin version.

Our analyses also suggest that the ACT parameterization, where the nucleation rate is linearly proportional to the H_2SO_4 concentration, performs reasonably well for the CARES location and time period. However, sensitivity studies such as those employing uncertainty quantification (UQ) techniques are needed that adjust empirical coefficients to better reproduce the observed growth rate of ultrafine particles and loss of particles through coagulation and condensation, and consequently the magnitude of total PNC over California. Since the aerosol size distribution is another source of uncertainty in models, additional studies testing the sensitivity of the size distribution to primary particle emissions may also improve the simulated particle number concentration and size distribution. Although the CARES campaign provided data to test and evaluate different new particle formation parameterizations, additional measurements such as H_2SO_4 and organic acid gas concentrations are necessary to better constrain the nucleation rate expressions.

Acknowledgements:

We thank the numerous scientists, pilots, and other staff that contributed to the data collection during CARES. CARES was supported by the U.S. Department of Energy's (DOE) Atmospheric Radiation Measurement (ARM) and Atmospheric System Research (ASR) programs. Funding for this research was provided by the U.S. NOAA's Atmospheric Composition and Climate Program (NA11OAR4310160) and utilized resources provided by the Pacific Northwest National Laboratory (PNNL) Institutional Computing program. PNNL is operated for the U.S. DOE by Battelle Memorial Institute.

References

Andreae, M.O., Rosenfeld, D.: Aerosol–cloud–precipitation interactions. Part 1. The nature and sources of cloud-active aerosols, Earth-Science Reviews, Volume 89, Issues 1–2, 13–41, 2008.

Archer-Nicholls, S., Lowe, D., Utembe, S., Allan, J., Zaveri, R. A., Fast, J. D., Hodnebrog, Ø., Denier van der Gon, H., and McFiggans, G.: Gaseous chemistry and aerosol mechanism developments for version 3.5.1 of the online regional model, WRF-Chem, Geosci. Model Dev., 7, 2557-2579, doi:10.5194/gmd-7-2557-2014, 2014.

Asmi, E., Kivekas, N., Kerminen, V.-M., Komppula, M., Hyvarinen, A.-P., Hatakka, J., Viisanen, Y. & Lihavainen, H.: Secondary new particle formation in Northern Finland Pallas site between the years 2000 and 2010, Atmos. Chem. Phys., 11, 12959–12972, doi:10.5194/acp-11-12959-2011, 2011.

Betha, R., Spracklen, D.V., Balasubramanian, R.: Observations of new aerosol particle formation in a tropical urban atmosphere, Atmos. Environ., 71, 340–351, http://dx.doi.org/10.1016/j.atmosenv.2013.01.049, 2013.

Boulon, J., Sellegri, K., Hervo, M., Picard, D., Pichon, J.-M., Fréville, P., and Laj, P.: Investigation of nucleation events vertical extent: a long term study at two different altitude sites, Atmos. Chem. Phys., 11, 5625–5639, doi:10.5194/acp-11-5625-2011, 2011.

Boy, M., Karl, T., Turnipseed, A., Mauldin, R.L, Kosciuch, E., Greenberg, J., Rathbone, J., Smith, J., Held, A., Barsanti, K., Wehner, B., Bauer, S., Wiedensohler, A., Bonn, B., Kulmala, M., and Guenther, A.: New particle formation in the Front Range of the Colorado Rocky Mountains, Atmos. Chem. Phys., 8, 1577–1590, 2008.

Carter, W.P.L.:. Implementation of the SAPRC-99 chemical mechanism into the models-3 framework. Report to the United States Environmental Protection Agency (http://www.cert.ucr.edu/~carter/absts.htm#s99mod3), 2000.

Cui, Y. Y., Hodzic, A., Smith, J.N., Ortega, J., Brioude, J., Matsui, H., Turnipseed, A., Winkler, P., and de Foy, B.: Modeling ultrafine particle growth at a pine forest site influenced by anthropogenic pollution during BEACHON-RoMBAS 2011, Atmos. Chem. Phys., 14, 11011-11029, doi:10.5194/acp-14-11011-2014, 2014.

Ehn, M., Thornton, J. A., Kleist, E., Sipilä, M., Junninen, H., Pullinen, I., Springer, M., Rubach, F., Tillmann, R., Lee, B., Lopez-Hilfiker, F., Andres, S., Acir, I.-H., Rissanen, M., Jokinen, T., Schobesberger, S., Kangasluoma, J., Kontkanen, J., Nieminen, T., Kurten, T., Nielsen, L. B., Jorgensen, S., Kjaergaard, H. G., Canagaratna, M., Maso, M. D., Berndt, T., Petaja, T., Wahner, A., Kerminen, V.-M., Kulmala, M., Worsnop, D. R., Wildt, J., and Mentel, T. F.: A large source of low-volatility secondary organic aerosol, Nature, 506, 476–479, doi:10.1038/nature13032, 2014.

Emmons, L. K., Walters, S., Hess, P. G., Lamarque, J.-F., Pfister, G. G., Fillmore, D., Granier, C., Guenther, A., Kinnison, D., Laepple, T., Orlando, J., Tie, X., Tyndall, G., Wiedinmyer, C., Baughcum, S. L., and Kloster, S.: Description and evaluation of the Model for Ozone and Related chemical Tracers, version 4 (MOZART-4), Geosci. Model Dev., 3, 43-67, 2010.

Fast, J.D., Gustafson, Jr, W.I., Easter, Jr, R.C., Zaveri, R.A., Barnard, J.C., Chapman, E.G., Grell, G., and Peckham, S.E.: Evolution of Ozone, Particulates, and Aerosol Direct Radiative Forcing in the Vicinity of Houston Using a Fully Coupled Meteorology-Chemistry-Aerosol Model, J. Geophys. R. D. (Atmospheres) 111 (D21): D21305. doi:10.1029/2005JD006721, 2006.

Fast, J.D., Gustafson Jr., W. I., Berg, L. K., Shaw, W. J., Pekour, M., Shrivastava, M., Barnard, J. C., Ferrare, R. A., Hostetler, C. A., Hair, J. A., Erickson, M.,B., Jobson, T., Flowers, B., Dubey, M.K., Springston, S., Pierce, R. B., , Dolislager, L., Pederson, J., and Zaveri, R. A.: Transport and mixing patterns over Central California during the carbonaceous aerosol and radiative effects study (CARES), Atmos. Chem. Phys., 12, 1759–1783, doi:10.5194/acp-12-1759-2012, 2012.

Fast, J. D., Allan, J., Bahreini, R., Craven, J., Emmons, L., Ferrare, R., Hayes, P. L., Hodzic, A., Holloway, J., Hostetler, C., Jimenez, J. L., Jonsson, H., Liu, S., Liu, Y., Metcalf, A., Middlebrook, A., Nowak, J., Pekour, M., Perring, A., Russell, L., Sedlacek, A., Seinfeld, J., Setyan, A., Shilling, J., Shrivastava, M., Springston, S., Song, C., Subramanian, R., Taylor, J. W., Vinoj, V., Yang, Q., Zaveri, R. A., and Zhang, Q.: Modeling regional aerosol and aerosol precursor variability over California and its sensitivity to emissions and long-range transport during the 2010 CalNex and CARES

campaigns, Atmos. Chem. Phys., 14, 10013–10060, doi:10.5194/acp-14-10013-2014, 2014.

Fuchs, N. and A. Sutugin,: High-dispersed aerosols, in Topics in Current Aerosol Research,edited by: G. M. Hidy and J. R. Brock,Pergamon, Oxford, UK, 2, 1–60, 1971

Grell, G. A., Peckham, S. E., Schmitz, R., McKeen, S. A., Frost, G., Skamarock, W. C., and Eder, B.: Fully coupled online chemistry within the WRF model, Atmos. Environ., 39, 6957-6975, 2005.

Guenther, A., Karl, T., Harley, P., Wiedinmyer, C., Palmer, P. I., and Geron, C.: Estimates of global terrestrial isoprene emissions using MEGAN (Model of Emissions of Gases and Aerosols from Nature), Atmos. Chem. Phys., 6, 3181–3210, doi:10.5194/acp-6-3181-2006, 2006.

Hoppel, W. A., Frick, G. M., Fitzgerald, J. W., and Larson, R. E.: Marine boundary layer measurements of new particle formation and the effects nonprecipitating clouds have on aerosol size distribution, J. Geophys. Res., 99, 14,443–14,459, 1994.

Iacono, M. J., Delamere, J. S., Mlawer, E. J., Shephard, M. W., Clough, S. A., and Collins, W. D.: Radiative forcing by long-lived greenhouse gases: Calculations with the AER radiative transfer models, J. Geophys. Res., 113, D13103, doi:10.1029/2008JD009944, 2008.

IPCC: 2007 - Denman, K.L., G. Brasseur, A. Chidthaisong, P. Ciais, P.M. Cox, R.E. Dickinson, D. Hauglustaine, C. Heinze, E. Holland, D. Jacob, U. Lohmann, S Ramachandran, P.L. da Silva Dias, S.C. Wofsy and X. Zhang: Couplings Between Changes in the Climate System and Biogeochemistry. In: Climate Change 2007: The Physical Science Basis. Contribution of Working Group I to the Fourth Assessment Report of the Intergovernmental Panel on Climate Change [Solomon, S., D. Qin, M. Manning, Z. Chen, M. Marquis, K.B. Averyt, M.Tignor and H.L. Miller (eds.)]. Cambridge University Press, Cambridge, United Kingdom and New York, NY, USA, 2007.

IPCC 2013 - Boucher, O., D. Randall, P. Artaxo, C. Bretherton, G. Feingold, P. Forster, V.-M. Kerminen, Y. Kondo, H. Liao, U. Lohmann, P. Rasch, S.K. Satheesh, S.

Sherwood, B. Stevens and X.Y. Zhang: Clouds and Aerosols. In: Climate Change 2013: The Physical Science Basis. Contribution of Working Group I to the Fifth Assessment Report of the Intergovernmental Panel on Climate Change [Stocker, T.F., D. Qin, G.-K. Plattner, M. Tignor, S.K. Allen, J. Boschung, A. Nauels, Y. Xia, V. Bex and P.M. Midgley (eds.)]. Cambridge University Press, Cambridge, United Kingdom and New York, NY, USA, 2013.

Janjic, Z. I.: Nonsingular Implementation of the Mellor-Yamada Level 2.5 Scheme in the NCEP Meso model. NCEP Office Note No. 437, 61 pp, 2001.

Jeong, C.H., Evans, G.J., McGuire, M.L., Chang, R.Y.-W., Abbatt, J.P.D., Zeromskiene, K., Mozurkewich, M., Li, S.M. and Leaitch, W.R.: Particle Formation and Growth at Five Rural and 20 Urban Sites. Atmos. Chem. Phys. 10: 7979–7995, doi: 10.5194/acp-10-7979-2010, 2010.

Jeong, C.H., Hopke, P.K., Chalupa, D., Utell, M.: Characteristics of nucleation and growth events of ultrafine particles measured in Rochester, NY. Environ. Sci. Technol. 38, 1933-1940, 2004.

Jokinen, T.,Berndt, T., Makkonen, R., Kerminen, V-M., Junninen, H.,Paasonen,P., Stratmann, F., Hermann, H., Guenther, A., Worsnop, D.R.,Kulmala, M., Ehn, M., Sipilä, M.: Production of extremely low volatile organic compounds from biogenic emissions: Measured yields and atmospheric implications, Proc. Nat. Acad. Sci., Vol. 112, No. 23, pp. 7123-7128, doi:10.1073/pnas.1423977112, 2015.

Jung, J., Fountoukis, C., Adams, P. J., and Pandis, S. N.: Simulation of in situ ultrafine particle formation in the eastern United States using PMCAMx-UF, J. Geophys. Res., 115, D03203, doi:10.1029/2009JD012313, 2010.

Jung, J. G., Pandis, S. N., Adams, P. J.: Evaluation of Nucleation Theories in a Sulfur-Rich Environment, Aerosol Science and Technology, 42, 7, 495-504, DOI:10.1080/02786820802187085, 2008.

Kain, J. S.: The Kain–Fritsch Convective Parameterization: An Update. J. Appl. Meteor., 43, 170–181. doi:http://dx.doi.org/10.1175/1520-0450(2004)043 , 2004.

Kazil, J., Harrison, R. G., and Lovejoy, E. R.: Tropospheric new particle formation and the role of ions, Space Sci. Rev., 137, 241–255, 2008.

Kerminen, V.-M.,, M. Paramonov, T. Anttila, I. Riipinen, C. Fountoukis, H. Korhonen, E. Asmi, L. Laakso, H. Lihavainen, E. Swietlicki, B. Svenningsson, A. Asmi, S. N. Pandis, M. Kulmala, and T. Petaja: Cloud condensation nuclei production associated with atmospheric nucleation: a synthesis based on existing literature and new results, Atmos. Chem. Phys., 12, 12037–12059, 2012, doi:10.5194/acp-12-12037-2012, 2012.

Kerminen, V.-M., and Kulmala, M.: Analytical Formulae Connecting the "Real" and the "Apparent" Nucleation Rate and the Nuclei Number Concentration for Atmospheric Nucleation Events, J. Aerosol Sci. 33:609–62, 2002.

Kirkby, J., Curtius, J., Almeida, J., Dunne, E., Duplissy, J., Ehrhart, S., Franchin, A., Gagné, S., Ickes, L., Kürten, A., Kupc, A., Metzger, A., Riccobono, F., Rondo, L., Schobesberger, S., Tsagkogeorgas, G., Wimmer, D., Amorim, A., Bianchi, F., Breitenlechner, M., David, A., Dommen, J., Downard, A., Ehn, M., Flagan, R. C., Haider, S., Hansel, A., Hauser, D. Jud, W., Junninen, H., Kreissl, F., Kvashin, A., Laaksonen, A., Lehtipalo, K., Lima, J., Lovejoy, E. R., Makhmutov, V., Mathot, S., Mikkilä, J., Minginette, P., Mogo, S., Nieminen, T., Onnela, A., Pereira, P., Petäjä, T., Schnitzhofer, R., Seinfeld, J. H., Sipilä, M., Stozhkov, Y., Stratmann, F., Tomé, A., Vanhanen, J., Viisanen, Y., Vrtala, A., Wagner, P. E., Walther, H., Weingartner, E., Wex, H., Winkler, P. M., Carslaw, K. S., Worsnop, D. R., and Kulmala, M.: Role of sulphuric acid, ammonia and galactic cosmic rays in atmospheric aerosol nucleation, Nature 476, 429–433, doi:10.1038/nature10343, 2011.

Kristensson, A., Dal Maso, M., Swietlicki, E., Hussein, T., Zhou, J., Kerminen, V.-M., and Kulmala, M.: Characterization of new particle formation events at a background site in Southern Sweden: relation to air mass history, Tellus, 60B, 330–344, DOI: 10.1111/j.1600-0889.2008.00345, 2008.

Kuang, C., McMurry, P. H., McCormick, A. V., and Eisele, F. L.: Dependence of nucleation rates on sulfuric acid concentration in diverse atmospheric locations, J. Geophys. Res., 113, D10, DOI: 10.1029/2007JD009253, 2008.

Kuang, C., McMurry, P.H., and McCormick, A.V.: Determination of cloud condensation nuclei production from measured new particle formation events, Geophys. Res. Lett., 36(L09822), doi:10.1029/2009GL037584, 2009.

Kuang, C., Riipinen, I., Sihto, S. L., Kulmala, M., McCormick, A. V., and McMurry, P. H.: An improved criterion for new particle formation in diverse atmospheric environments, Atmos. Chem. Phys., 10 (17), 8469–8480, doi:10.5194/acp-10-8469-2010, 2010.

Kuang, C., Chen, M., Zhao, J., Smith, J., McMurry, P. H., and Wang, J.: Size and time-resolved growth rate measurements of 1 to 5 nm freshly formed atmospheric nuclei, Atmos. Chem. Phys., 12(7), 3573–3589, doi:10.5194/acp-12-3573-2012, 2012.

Kulmala, M., Lehtinen, K. E. J., and Laaksonen, A.: Cluster activation theory as an explanation of the linear dependence between formation rate of 3 nm particles and sulphuric acid concentration, Atmos. Chem. Phys., 6, 787–793, 2006.

Kulmala, M., Laaksonen, A., and Pirjola, L.: Parameterizations for sulphuric acid/water nucleation rates, J. Geophys. Res.,103, 8301–8307, doi:10.1029/97JD03718, 1998.

Kuwata, M., Kondo, Y., Miyazaki, Y., Komazaki, Y., Kim, J. H., Yum, S. S., Tanimoto, H., and Matsueda, H.: Cloud condensation nuclei activity at Jeju Island, Korea in spring 2005, Atmos. Chem. Phys., 8, 2933-2948, doi:10.5194/acp-8-2933-2008, 2008.

Lee, Y. H., Pierce, J. R., and Adams, P. J.: Representation of nucleation mode microphysics in a global aerosol model with sectional microphysics, Geosci. Model Dev., 6, 1221-1232, doi:10.5194/gmd-6-1221-2013, 2013.

Levin, E. J. T., Prenni, A. J., Petters, M. D., Kreidenweis, S. M., Sullivan, R. C., Atwood, S. A., Ortega, J., DeMott, P. J., and Smith, J. N.: An annual cycle of size-resolved aerosol hygroscopicity at a forested site in Colorado, J. Geophys. Res., 117, 06201, doi:10.1029/2011JD016854, 2012.

Matsui, H., Koike, M., Kondo, Y., Takegawa, N., Wiedensohler, A., Fast, J. D., and Zaveri, R. A.: Impact of new particle formation on the concentrations of aerosols and cloud condensation nuclei around Beijing, J. Geophys. R., Vol. 116, D19208, doi:10.1029/2011JD016025, 2011.

Matsui, H., Koike, M., Takegawa, N., Kondo, Y., Takami, A., Takamura, T., Yoon, S., Kim, S.-W., Lim, H.-C., and Fast, J. D.: Spatial and temporal variations of new particle formation in East Asia using an NPF-explicit WRF-chem model: North-south contrast in new particle formation frequency, J. Geophys. Res. Atmos., 118, 11,647–11,663, doi:10.1002/jgrd.50821, 2013.

Makkonen, R., Asmi, A., Korhonen, H., Kokkola, H., Jarvenoja, S.,Raisanen, P., Lehtinen, K. E. J., Laaksonen, A., Kerminen, V.-M., Jarvinen, H., Lohmann, U., Bennartz, R., Feichter, J., and Kulmala, M.: Sensitivity of aerosol concentrations and cloud properties to nucleation and secondary organic distribution in ECHAM5-HAM global circulation model, Atmos. Chem. Phys., 9, 1747–1766, doi:10.5194/acp-9-1747-2009, 2009.

McMurry, P. H.: Photochemical aerosol formation from SO_2: A theoretical analysis of smog chamber data, J. Colloid Interface Sci., 78, 513–527, doi:10.1016/0021-9797(80)90589-5, 1980.

McMurry, P. H., and Friedlander, S. K.: New particle formation in the presence of an aerosol, Atmospheric Environment, 13, 1635-1651, 1979.

McMurry, P. H., Woo, K. S., Weber, R., Chen, D.- R., and Pui, D. Y. H.: Size distributions of 3–10 nm atmospheric particles: Implications for nucleation mechanisms, Philos. Trans. R. Soc., Ser. A,358, 2625–2642, doi:10.1098/rsta.2000.0673, 2000.

Mei, F., Setyan, A., Zhang, Q., and Wang, J.: CCN activity of organic aerosols observed downwind of urban emissions during CARES, Atmos. Chem. Phys., 13, 12155-12169, doi:10.5194/acp-13-12155-2013, 2013.

Merikanto, J., Napari, I., Vehkamäki, H., Anttila, T., and Kulmala, M.: New parameterization of sulfuric acid- ammonia- water ternary nucleation rates at tropospheric conditions, J. Geophys. Res., 112, D15207, doi:10.1029/2006JD007977, 2007.

Merikanto, J., Spracklen, D. V., Mann, G. W., Pickering, S. J., and Carslaw, K. S.: Impact of nucleation on global CCN, Atmos. Chem. Phys., 9, 8601-8616, doi:10.5194/acp-9-8601-2009, 2009.

Metzger, A., Verheggen, B., Dommen, J., Duplissy, J., Prevot, A. S., Weingartner, E., Riipinen, I., Kulmala, M., Spracklen, D. V., Carslaw, K. S., and Baltensperger, U.: Evidence for the role of organics in aerosol particle formation under atmospheric conditions, Proc. Nat. Acad. Sci., 107, doi:10.1073/pnas.0911330107, 2010.

Morrison, H., Thompson, G., and Tatarskii, V.: Impact of cloud microphysics on the development of trailing stratiform precipitation in a simulated squall line: comparison of one- and two-moment schemes. Monthly Weather Review, 137, 991–1007, doi:10.1175/2008MWR2556.1, 2009.

Napari, I., Noppel, M., Vehkamäki, H., and Kulmala, M.: Parameterization of ternary nucleation rates for H_2SO_4-NH_3−H_2O vapors, J. Geophys. Res., 107 (D19), 4381, doi:10.1029/2002JD002132, 2002.

O'Dowd, C.D., Hoffman, T.: Coastal new particle formation: a review of the current state-of-the-art. Environ. Chem., 2, 245-255. http:// dx.doi.org/10.1071/EN05077, 2005.

Paasonen, P., Nieminen, T., Asmi, E., Manninen, H. E., Petaja, T., Plass-Dulmer, C., Flentje, H., Birmili, W., Wiedensohler, A., Ñorrak, U., Metzger, A., Hamed, A., Laaksonen, A., Facchini, M. C., Kerminen, V.-M., and Kulmala, M.: On the roles of sulphuric acid and low-volatility organic vapours in the initial steps of atmospheric new particle formation, Atmos. Chem. Phys., 10, 11223–11242, doi:10.5194/acp-10-11223-2010, 2010.

Patoulias, D., Fountoukis, C., Riipinen, I., and Pandis, S. N.: The role of organic condensation on ultrafine particle growth during nucleation events, Atmos. Chem. Phys., 15, 6337-6350, doi:10.5194/acp-15-6337-2015, 2015.

Pierce, J.R., Leaitch, W. R., Liggio, J., Westervelt, D. M., Wainwright, C. D., Abbatt, J. P. D., Ahlm, L., Al-Basheer, W., Cziczo, D. J., Hayden, K. L., Lee, A. K. Y., Li, S.-M., Russell, L. M., Sjostedt, S. J., Strawbridge, K. B., Travis, M., Vlasenko, A., Wentzell, J. J. B., Wiebe, H. A., Wong, J. P. S., and Macdonald, A. M.: Nucleation and condensational growth to CCN sizes during a sustained pristine biogenic SOA event in a forested mountain valley, Atmos. Chem. Phys., 12, 3147–3163, 2012, doi:10.5194/acp-12-3147-2012, 2012.

Pierce, J. R., Riipinen, I., Kulmala, M., Ehn, M., Petäjä, T., Junninen, H., Worsnop, D. R., and Donahue, N. M.: Quantification of the volatility of secondary organic compounds in ultrafine particles during nucleation events, Atmos. Chem. Phys., 11, 9019-9036, doi:10.5194/acp-11-9019-2011, 2011.

Pierce, J. R. and Adams, P. J.: Uncertainty in global CCN concentrations from uncertain aerosol nucleation and primary emission rates, Atmos. Chem. Phys., 9, 1339–1356, doi:10.5194/acp-9- 1339-2009, 2009.

Place, P. F., Jr., Ziemba, L.D., and Griffin, R.J.: Observations of nucleation-mode particle events and size distributions at a rural New England site, Atmos. Environ., 44, 88-94, 2010.

Reddington, C. L., Carslaw, K. S., Spracklen, D. V., Frontoso, M. G., Collins, L., Merikanto, J., Minikin, A., Hamburger, T., Coe, H., Kulmala, M., Aalto, P., Flentje, H., Plass-Dulmer, C., Birmili, W., Wiedensohler, A., Wehner, B., Tuch, T., Sonntag, A., O'Dowd, C. D., Jennings, S. G., Dupuy, R., Baltensperger, U., Weingartner, E., Hansson, H.-C., Tunved, P., Laj, P., Sellegri, K., Boulon, J., Putaud, J.-P., Gruening, C., Swietlicki, E., Roldin, P., Henzing, J. S., Moerman, M., Mihalopoulos, N., Kouvarakis, G., Zdimal, V., Zikova, N., Marinoni, A., Bonasoni, P., and Duchi, R.: Primary versus secondary contributions to particle number concentrations in the European boundary layer Atmos. Chem. Phys., 11, 12007–12036, doi:10.5194/acp-11-12007-2011, 2011.

Riccobono, F., Schoberberger, S., Scott, C. E., Dommen, J., Ortega, I. K., Rondo, L., Almeida, J., Amorim, A., Bianchi, F., Breitenlechner, M., David, A., Downard, A., Dunne, E. M., Duplissy, J., Ehrhardt, S., Flagan, R. C., Franchin, A., Hansel, A., Juuninen, H., Kajos, M., Keskinen, H., Kupc, A., Kürten, A., Kvashin, A. N., Laaksonen, A., Lehtipalo, K., Makkmutov, V., Mathot, S., Nieminen, T., Onnela, A., Petäjä, T.,Praplan, A. P., Santos, F. D., Schallhart, S., Seinfeld, J. H., Sipilä, M., Spracklen, D. V., Stozhkov, Y., Stratmann, F., Tomé, A., Tsagkogeorgas, G., Vaattlovaara, P., Viisanen, Y., Vrtala, A., Wagner, P. E., Weingartner, E., Wex, H., Wimmer, D., Carslaw, K. S., Curtius, J., Donahue, N. M., Kirkby, J., Kulmala, M. Worsnop, D. R., and Baltensperger, U.: Oxidation products of biogenic emissions contribute to nucleation of atmospheric particles, Science, 344, 717–721, 2014.

Riipinen, I., Pierce, J. R., Yli-Juuti, T., Nieminen, T., Häkkinen, S., Ehn, M., Junninen, H., Lehtipalo, K., Petäjä, T., Slowik, J., Chang, R., Shantz, N. C., Abbatt, J., Leaitch, W. R., Kerminen, V.-M., Worsnop, D. R., Pandis, S. N., Donahue, N. M., and Kulmala, M.: Organic condensation: a vital link connecting aerosol formation to cloud condensation nuclei (CCN) concentrations, Atmos. Chem. Phys., 11, 3865–3878, doi:10.5194/acp-11-3865-2011, 2011.

Riipinen, I., Sihto, S.-L., Kulmala, M., Arnold, F., Dal Maso, M., Birmili, W., Saarnio, K., Teinilä, K., Kerminen, V.-M., Laaksonen, A., and Lehtinen, K. E. J.: Connections between atmospheric sulphuric acid and new particle formation during QUEST III–IV campaigns in Heidelberg and Hyytiälä, Atmos. Chem. Phys., 7, 1899-1914, doi:10.5194/acp-7-1899-2007, 2007.

Ritter, M., Müller, M. D., Tsai, M.-Y., and Parlow, E.: Air pollution modeling over very complex terrain: an evaluation of WRF-Chem over Switzerland for two 1-year periods, Atmos. Res., 132–133, 209–222, 2013.

Sem, G. J.: Design and performance characteristics of three continuous-flow condensation particle counters: a summary, Atmos. Res., 62, 267–294, doi:10.1016/S0169-8095(02)00014-5, 2002.

Setyan, A., Zhang, Q., Merkel, M., Knighton, W. B., Sun, Y., Song, C., Shilling, J. E., Onasch, T. B., Herndon, S. C., Worsnop, D. R., Fast, J. D., Zaveri, R. A., Berg, L. K., Wiedensohler, A., Flowers, B. A., Dubey, M. K., and Subramanian, R.: Characterization of submicron particles influenced by mixed biogenic and anthropogenic emissions using high-resolution aerosol mass spectrometry: results from CARES, Atmos. Chem. Phys., 12, 8131-8156, doi:10.5194/acp-12-8131-2012, 2012.

Setyan, A., Song, C., Merkel, M., Knighton, W. B., Onasch, T. B., Canagaratna, M. R., Worsnop, D. R., Wiedensohler, A., Shilling, J. E., and Zhang, Q.: Chemistry of new particle growth in mixed urban and biogenic emissions – insights from CARES, Atmos. Chem. Phys., 14, 6477-6494, doi:10.5194/acp-14-6477-2014, 2014.

Schobesberger, S., Junninen, H., Bianchi, F., Lönn, G., Ehn, M., Lehtipalo, K., Dommen, J., Ehrhart, S., Ortega, I. K., Franchin, A., Nieminen, T., Riccobono, F., Hutterli, M.,

Duplissy, J., Almeida, J., Amorim, A., Breitenlechner, M., Downard, A. J., Dunne, E. M., Flagan, R. C., Kajos, M., Keskinen, H., Kirkby, J.,Kupc, A., Kürten, A., Kurtén, T., Laaksonen, A., Mathot, S., Onnela, A., Praplan, A. P., Rondo, L., Santos, F. D., Schallhart, S., Schnitzhofer, R., Sipilä, M., Tomé, A., Tsagkogeorgas, G., Vehkamäki, H., Wimmer, D., Baltensperger, U., Carslaw, K. S., Curtius, J., Hansel, A., Petäjä, T., Kulmala, M., Donahue, N. M., and Worsnop, D. R.: Molecular understanding of atmospheric particle formation from sulfuric acid and large oxidized organic molecules, Proc. Natl. Acad. Sci. USA, 110, 17223-17228, 10.1073/pnas.1306973110, 2013.

Shaw, W., Allwine, K. J., Fritz, B. G., Rutz, F. C., Rishel, J. P., and Chapman, E. G.: An evaluation of the wind erosion module in DUSTRAN, Atmos. Environ., 42, 1907–1921, 2008.

Shrivastava, M.K.B., Easter, R.C., Liu, X., Zelenyuk, A., Singh, B., Zhang, K.,Ma, P.L., Chand, D., Ghan, S.J., Jiminez, J.L., Zhang, Q., Fast, J.D., Rasch, P.J., and Tiitta, P.: Global transformation and fate of SOA: Implications of Low Volatility SOA and Gas-Phase Fragmentation Reactions, J. Geophys. Res. D. (Atmospheres) 120(9):4169-4195, doi:10.1002/2014JD022563, 2015.

Shrivastava, M., A. Zelenyuk, D. Imre, R. Easter, J. Beranek, R. A. Zaveri, and J. Fast: Implications of low volatility SOA and gas-phase fragmentation reactions on SOA loadings and their spatial and temporal evolution in the atmosphere, J. Geophys. Res.-Atmos., 118(8), 3328-3342, 2013.

Shrivastava, M., Fast, J., Easter, R., Gustafson Jr., W. I., Zaveri, R. A., Jimenez, J. L., Saide, P., and Hodzic, A.: Modeling organic aerosols in a megacity: comparison of simple and complex representations of the volatility basis set approach, Atmos. Chem. Phys., 11(13), 6639-6662, 2011.

Sihto, S.-L., Mikkilä, J., Vanhanen, J., Ehn, M., Liao, L., Lehtipalo, K., Aalto, P. P., Duplissy, J., Petäjä, T., Kerminen, V.-M., Boy, M., and Kulmala, M.: Seasonal variation of CCN concentrations and aerosol activation properties in boreal forest, Atmos. Chem. Phys., 11, 13269-13285, doi:10.5194/acp-11-13269-2011, 2011.

Sihto, S.-L., Kulmala, M., Kerminen, V.-M., Dal Maso, M., Petaja, T., Riipinen, I., Korhonen, H.,Arnold, F., Janson, R., Boy, M., Laaksonen, A., and Lehtinen, K. E. J.: Atmospheric sulphuric acid and aerosol formation: implications from atmospheric measurements for nucleation and early growth mechanisms, Atmos. Chem. Phys., 6, 4079–4091,doi:10.5194/acp-6-4079-2006, 2006.

Smith, J. N., Dunn, M. J., VanReken, T. M., Iida, K., Stolzenburg, M. R., McMurry, P. H., and Huey, L. G.: Chemical composition of atmospheric nanoparticles formed from nucleation in Tecamac, Mexico: Evidence for an important role for organic species in nanoparticle growth, Geophys. Res. Lett., 35, L04808, doi:10.1029/2007GL032523, 2008.

Spracklen, D.V., Pringle, K. J., Carslaw, K. S., Chipperfield, M. P., and Mann, G. W.: A global off-line model of size-resolved aerosol microphysics: I. Model development and prediction of aerosol properties, Atmos. Chem. Phys., 5, 2227–2252, 2005.

Spracklen, D. V., Carslaw, K. S., Kulmala, M., Kerminen, V.-M., Mann, G. W., and Sihto, S.-L.: The contribution of boundary layer nucleation events to total particle concentrations on regional and global scales, Atmos. Chem. Phys., 6, 5631–5648, 2006.

Spracklen, D. V., Carslaw, K. S., Kulmala, M., Kerminen, V.-M., Sihto, S.-L., Riipinen, I., Merikanto, J., Mann, G. W., Chipperfield,M. P., Wiedensohler, A., Birmili, W., and Lihavainen, H.: Contribution of particle formation to global cloud condensation nuclei concentrations, Geophys. Res. Lett., 35, L06808, doi:10.1029/2007GL033038, 2008.

Spracklen, D. V., Carslaw, K. S., Merikanto, J., Mann, G. W., Reddington, C. L., Pickering, S., Ogren, J. A., Andrews, E., Baltensperger, U., Weingartner, E., Boy, M., Kulmala, M., Laakso, L., Lihavainen, H., Kivekas, N., Komppula, M., Mihalopoulos, N., Kouvarakis, G., Jennings, S. G., O'Dowd, C., Birmili, W., Wiedensohler, A., Weller, R., Gras, J., Laj, P., Sellegri, K., Bonn, B., Krejci, R., Laaksonen, A., Hamed, A., Minikin, A., Harrison, R. M., Talbot, R., and Sun, J.: Explaining global surface aerosol number concentrations in terms of primary emissions and particle formation, Atmos. Chem. Phys., 10, 4775-4793, doi:10.5194/acp-10-4775-2010, 2010.

Turco, R. P., Zhao, J.-X., and Yu, F.: A new source of tropospheric aerosols: Ion-ion recombination, Geophys. Res. Lett., 25, 635–638, doi:10.1029/98GL00253, 1998.

Vehkamäki, H., Kulmala, M., Napari, I., Lehtinen, K. E. J., Timmreck, C., Noppel, M., and Laaksonen, A.: An improved parameterization for sulfuric acid- water nucleation rates for tropospheric and stratospheric conditions, J. Geophys. Res., 107(D22), 4622, doi:10.1029/2002JD002184, 2002.

Venzac, H., Sellegri, K., Villani, P., Picard, D., and Laj, P.: Seasonal variation of aerosol size distributions in the free troposphere and residual layer at the puy de Dome station, France, Atmos. Chem. Phys., 9, 1465–1478, 2009.

Westervelt, D. M., Pierce, J. R., and Adams, P. J.: Analysis of feedbacks between nucleation rate, survival probability and cloud condensation nuclei formation, Atmos. Chem. Phys., 14, 5577-5597, doi:10.5194/acp-14-5577-2014, 2014.

Westervelt, D. M., Pierce, J. R., Riipinen, I., Trivitayanurak, W., Hamed, A., Kulmala, M., Laaksonen, A., Decesari, S., and Adams, P. J.: Formation and growth of nucleated particles into cloud condensation nuclei: model–measurement comparison, Atmos. Chem. Phys., 13, 7645-7663, doi:10.5194/acp-13-7645-2013, 2013.

Wexler, A. S., Lurmann, F. W., and Seinfeld, J. H.: Modeling urban and regional aerosols. I. Model development, Atmos. Environ., 28, 531–546, doi:10.1016/1352-2310(94)90129-5, 1994.

Wiedensohler, A, Chen, Y. F., Nowak, A, Wehner, B., Achtert, P, Berghof, M., Birmili, W., Wu, Z. J., Hu, M., Zhu, T., Takegawa, N., Kita, K., Kondo, Y., Lou, S. R., Hofzumahaus, A, Holland, F, Wahner, A., Gunthe, S. S., Rose, D., Su, H., and Poschl, U.: Rapid aerosol particle growth and increase of cloud condensation nucleus activity by secondary aerosol formation and condensation: A case study for regional air pollution in northeastern China, J. Geophys. Res., 114, 00G08, doi:10.1029/2008JD010884, 2009.

Yli-Juuti, T., Barsanti, K., Hildebrandt Ruiz, L., Kieloaho, A.-J., Makkonen, U., Petäjä, T., Ruuskanen, T., Kulmala, M., and Riipinen, I.: Model for acid-base chemistry in nanoparticle growth (MABNAG), Atmos. Chem. Phys., 13, 12507-12524, doi:10.5194/acp-13-12507-2013, 2013.

Yli-Juuti, T., Nieminen, T., Hirsikko, A., Aalto, P. P., Asmi, E., Hõrrak, U., Manninen, H. E., Patokoski, J., Dal Maso, M., Petäjä, T., Rinne, J., Kulmala, M., and Riipinen, I.: Growth rates of nucleation mode particles in Hyytiälä during 2003−2009: variation with particle size, season, data analysis method and ambient conditions, Atmos. Chem. Phys., 11, 12865-12886, doi:10.5194/acp-11-12865-2011, 2011.

Yu, F. and Turco, R. P.: Ultrafine aerosol formation via ion-mediated nucleation, Geophys. Res. Lett., 27, 883–886, 2000.

Yu, F. and Turco, R. P.: From molecular clusters to nanoparticles: Role of ambient ionization in tropospheric aerosol formation, J. Geophys. Res., 106, 4797–4814, 2001.

Yu, F., Wang, Z., Luo, G., and Turco, R.: Ion-mediated nucleation as an important global source of tropospheric aerosols, Atmos. Chem. Phys., 8, 2537-2554, 2008.

Yu, F.: A secondary organic aerosol formation model considering successive oxidation aging and kinetic condensation of organic compounds: global scale implications, Atmos. Chem. Phys., 11, 1083–1099, doi:10.5194/acp-11-1083-2011, 2011.

Yu, F., Luo, G., Pryor, S. C., Pillai, P. R., Lee, S. H., Ortega, J., Schwab, J. J., Hallar, A. G., Leaitch, W. R., Aneja, V. P., Smith, J. N., Walker, J. T., Hogrefe, O., and Demerjian, K. L.: Spring and summer contrast in new particle formation over nine forest areas in North America, Atmos. Chem. Phys. Discuss., 15, 21271-21298, doi:10.5194/acpd-15-21271-2015, 2015.

Yue, D. L., Hu, M., Zhang, R. Y., Wu, Z. J., Su, H., Wang, Z. B., Peng, J. F., He, L. Y., Huang, X. F., Gong, Y.G., and Wiedensohler, A.: Potential contribution of new particle formation to cloud condensation nuclei in Beijing, Atmos. Environ., 45(33), 6070–6077, 2011.

Zaveri, R.A., Easter, Jr, R.C., Fast, J.D., and Peters, L.K.: Model for Simulating Aerosol Interactions and Chemistry (MOSAIC). J. Geophys. R. D. (Atmospheres) 113(D13): Art. No. D13204. doi:10.1029/2007JD008782, 2008.

Zaveri, R. A., Shaw, W. J., Cziczo, D. J., Schmid, B., Ferrare, R. A., Alexander, M. L., Alexandrov, M., Alvarez, R. J., Arnott, W. P., Atkinson, D. B., Baidar, S., Banta, R. M., Barnard, J. C., Beranek, J., Berg, L. K., Brechtel, F., Brewer, W. A., Cahill, J. F.,

Cairns, B., Cappa, C. D., Chand, D., China, S., Comstock, J. M., Dubey, M. K., Easter, R. C., Erickson, M. H., Fast, J. D., Floerchinger, C., Flowers, B. A., Fortner, E., Gaffney, J. S., Gilles, M. K., Gorkowski, K., Gustafson, W. I., Gyawali, M., Hair, J., Hardesty, R. M., Harworth, J. W., Herndon, S., Hiranuma, N., Hostetler, C., Hubbe, J. M., Jayne, J. T., Jeong, H., Jobson, B. T., Kassianov, E. I., Kleinman, L. I., Kluzek, C., Knighton, B., Kolesar, K. R., Kuang, C., Kubátová, A., Langford, A. O., Laskin, A., Laulainen, N., Marchbanks, R. D., Mazzoleni, C., Mei, F., Moffet, R. C., Nelson, D., Obland, M. D., Oetjen, H., Onasch, T. B., Ortega, I., Ottaviani, M., Pekour, M., Prather, K. A., Radney, J. G., Rogers, R. R., Sandberg, S. P., Sedlacek, A., Senff, C. J., Senum, G., Setyan, A., Shilling, J. E., Shrivastava, M., Song, C., Springston, S. R., Subramanian, R., Suski, K., Tomlinson, J., Volkamer, R., Wallace, H. W., Wang, J., Weickmann, A. M., Worsnop, D. R., Yu, X.-Y., Zelenyuk, A., and Zhang, Q.: Overview of the 2010 Carbonaceous Aerosols and Radiative Effects Study (CARES), Atmos. Chem. Phys., 12, 7647-7687, doi:10.5194/acp-12-7647-2012, 2012.

Zaveri, R. A., Easter, R. C., Shilling, J. E., and Seinfeld, J. H.: Modeling kinetic partitioning of secondary organic aerosol and size distribution dynamics: representing effects of volatility, phase state, and particle-phase reaction, Atmos. Chem. Phys., 14, 5153-5181, doi:10.5194/acp-14-5153-2014, 2014.

Ziemba, L.D., Griffin, R.J., and Talbot, R.W.: Observations of elevated particle number concentration events at a rural site in northern New England, *J. Geophys. Res.*, 111, D23S24, doi:10.1029/2006JD007607, 2006.

Zhang, Y., Liu, P., Liu X.- H., Jacobson, M. Z., McMurry, P. H., Yu, F., Yu, S., and Schere, K. L.: A comparative study of nucleation parameterizations: 2. Three dimensional model application and evaluation, J. Geophys. Res., 115, D20213,doi:10.1029/2010JD014151, 2010a

Zhang, Y., McMurry, P. H., Yu, F., and Jacobson, M. Z.: A comparative study of nucleation parameterizations: 1. Examination and evaluation of the formulations, J. Geophys. Res., 115, D20212, doi:10.1029/2010JD014150, 2010b

Table 1. Observed mean and simulation summary statistics for aerosol number concentrations for particle diameters ≥ 10 nm (CN10), ≥ 40 nm (CN40), and ≥ 100 nm (CN100). The normalized mean bias (NMB) and correlation coefficient (R) are calculated between simulated and observed number concentration at the CARES T0 site during the June 7 -16, 2010 period.

Analyzed period	Observed mean			Model	NMB (%)			R		
	CN10	CN40	CN100	experiment	CN10	CN40	CN100	CN10	CN40	CN100
Entire period	8576	2748	366	ACT	184	66	78	0.71	0.56	0.53
				KIN	255	67	65	0.69	0.56	0.50
				ORG	233	71	68	0.66	0.57	0.51
				8BIN	-	-34	-55	-	0.56	0.32
South-westerly flow	9885	3328	435	ACT	191	60	86	0.71	0.53	0.45
				KIN	278	63	71	0.68	0.52	0.40
				ORG	228	66	75	0.67	0.54	0.40
				8BIN	-	-68	-47	-	0.15	0.53
Northerly flow	6162	1686	202	ACT	168	87	49	0.48	0.17	0.08
				KIN	193	83	47	0.41	0.16	0.07
				ORG	247	88	42	0.44	0.20	0.03
				8BIN	-	-66	-48	-	0.24	0.30

1 Table 2. Same as Table 1, except for the CARES T1 site

Analyzed period	Observed mean			Model experiment	NMB (%)			R		
	CN10	CN40	CN100		CN10	CN40	CN100	CN10	CN40	CN100
Entire period	6389	3121	518	ACT	178	31	25	0.74	0.70	0.51
				KIN	231	36	13	0.64	0.49	0.55
				ORG	239	36	16	0.67	0.69	0.51
				8BIN	-	-51	-65	-	0.57	0.32
South-westerly flow	7960	4073	691	ACT	187	35	33	0.71	066	0.33
				KIN	347	27	6	0.62	0.43	0.41
				ORG	256	41	23	0.59	0.63	0.32
				8BIN	-	-58	-62	-	0.51	0.03
Northerly flow	4429	1878	289	ACT	129	19	-12	0.67	0.11	-0.13
				KIN	278	68	7	0.41	0.06	0.07
				ORG	158	18	-16	0.68	0.10	-0.16
				8BIN	-	-40	-77	-	0.06	-0.16

2

Table 3. Selected budget diagnostic terms (cm^{-3} h^{-1}) for all NPE days at the T0 and T1 sites, averaged over 0400-1600 PST on each day. The CN1-10 Transport+Deposition term includes advection, turbulent mixing, and dry deposition.

NPE event	Experiment	CN1-10 Transport + Deposition	CN1-10 Condensation	CN1-10 Nucleation	CN1-10 Coagulation	CN10-100 Condensation + Coagulation
June 7, 2010	ACT	-467	-6165	64200	-56662	3113
	KIN	34589	-28112	568746	-566077	7851
	ORG	-111977	-34309	2295385	-2127692	8648
June 8, 2010	ACT	30028	-33002	493769	-498615	14378
	KIN	-706731	-43362	22285077	-21623692	11718
	ORG	-142762	-19701	1323769	-1147923	5311
June 9, 2010	ACT	13514	-44665	136923	-105308	37167
	KIN	-78154	-85439	1812308	-1646923	71408
	ORG	-163368	-56626	1868154	-1646000	44537
June 10,2010	ACT	38646	-53764	45238	-29546	50833
	KIN	7144	-80066	307523	-229331	78095
	ORG	-194592	-77118	630231	-352538	68368
June 11,	ACT	37617	-50877	25515	-11409	49099
2010	KIN	8629	-58040	100538	-51247	56856
	ORG	-282259	-84154	687231	-310454	68239
June 14,	ACT	25291	-31878	608846	-594692	10094
2010	KIN	-1036169	-50777	28470000	-27343923	18983
	ORG	-72954	-21925	900462	-797923	8930
June 15,	ACT	5769	-27877	267462	-243431	11901
2010	KIN	-418362	-25031	7323846	-7022969	25423
	ORG	-77023	-26138	1231000	-1129462	17232
June 16,	ACT	54250	-79367	84167	-56858	74135
2010	KIN	-159425	-49981	832727	-615400	46482
	ORG	-142382	-72017	425417	-207458	64203

Table 4. Observed mean and simulation summary statistics for aerosol number concentrations for particle diameters ≥ 3 nm (CN3) and CN10. The observed mean, normalized mean bias (NMB) and correlation coefficient (R) are calculated between simulated and observed number concentration collected during the CARES G-1 aircraft flights.

PNC	Flight	Observed mean	NMB(%)			R		
			ACT	KIN	ORG	ACT	KIN	ORG
CN3	June 8, morning (08a)	20472	157	614	227	0.64	0.67	0.74
	June 8, afternoon (08b)	13990	274	603	204	0.84	0.79	0.67
	June 10, morning (10a)	17392	212	365	212	0.22	0.19	-0.05
	June 12, morning (12a)	12340	198	162	243	0.40	0.29	0.50
	June 12, afternoon (12b)	14459	184	307	359	-0.06	0.10	0.32
	June 14, morning (14a)	21913	259	824	368	0.56	0.57	0.51
	June 15, morning (15a)	24800	250	845	296	0.68	0.69	0.61
	June 15, afternoon (15b)	14800	260	776	330	0.75	0.46	0.38
	All flights	17564	226	608	282	0.52	0.51	0.48
CN10	June 8, morning (08a)	11588	90	173	118	0.57	0.58	0.58
	June 8, afternoon (08b)	10161	162	219	168	0.80	0.81	0.77
	June 10, morning (10a)	10804	95	138	92	-0.03	0.03	-0.12
	June 12, morning (12a)	6019	69	105	87	0.44	0.49	0.55
	June 12, afternoon (12b)	7940	128	128	105	-0.05	-0.04	-0.04
	June 14, morning (14a)	11999	221	365	273	0.72	0.70	0.60
	June 15, morning (15a)	13601	216	338	250	0.71	0.70	0.61
	June 15, afternoon (15b)	12625	230	296	068	0.48	0.14	0.29
	All flights	10641	162	239	184	0.54	0.51	0.49

Table 5. Summary statistics for CCN number concentration at several super saturations (SS = 0.1%, 0.2%, 0.35%, 0.5%). The observed mean, normalized mean bias (NMB) and correlation coefficient (R) are calculated between simulated and observed number concentration at the T0 site during the June 7 - 16, 2010 period.

Observed mean				Experiment	NMB(%)				R			
$SS_{0.1}$	$SS_{0.2}$	$SS_{0.35}$	$SS_{0.5}$		$SS_{0.1}$	$SS_{0.2}$	$SS_{0.35}$	$SS_{0.5}$	$SS_{0.1}$	$SS_{0.2}$	$SS_{0.35}$	$SS_{0.5}$
105	329	729	1067	ACT	-49	-34	-5	29	0.39	0.23	0.39	0.30
				KIN	-49	-34	-9	27	0.39	0.22	0.35	0.28
				ORG	-49	-33	-8	26	0.38	0.23	0.36	0.29

Table 6. Same as Table 5, except for the T1 site

Observed mean				Experiment	NMB(%)				R			
$SS_{0.1}$	$SS_{0.2}$	$SS_{0.35}$	$SS_{0.5}$		$SS_{0.1}$	$SS_{0.2}$	$SS_{0.35}$	$SS_{0.5}$	$SS_{0.1}$	$SS_{0.2}$	$SS_{0.35}$	$SS_{0.5}$
109	333	729	1181	ACT	-53	-29	6	26	0.62	0.40	0.43	0.58
				KIN	-53	-32	-1	22	0.64	0.39	0.40	0.57
				ORG	-52	-33	1	23	0.63	0.40	0.41	0.58

Table 7. Summary statistics for CN10, CN40 and CN100 when using the ACT parameterization in a sectional framework with different numbers of particle size bins together with statistics for default configuration of WRF-Chem (WEX-8BIN). It should be noted that WEX-8BIN statistical results are the same as the 8BIN simulation presented in Tables 1 and 2. The observed mean, normalized mean bias (NMB) and correlation coefficient (R) are calculated between simulated and observed number concentration at the T0 site during the June 7 - 16, 2010 period

Observed mean			Experiment	NMB(%)			R		
CN10	CN40	CN100		CN10	CN40	CN100	CN10	CN40	CN100
8576	2748	366	WEX-8BIN	-	-34	-55	-	0.56	0.32
			ACT-8BIN	-	-8	-58	-	0.32	0.24
			ACT-12BIN	188	18	49	0.72	0.46	0.48
			ACT-20BIN	184	66	78	0.71	0.56	0.53

Table 8. Same as Table 7, except for the T1 site

Observed mean			Experiment	NMB(%)			R		
CN10	CN40	CN100		CN10	CN40	CN100	CN10	CN40	CN100
6389	3121	518	WEX-8BIN	-	-51	-65	-	0.57	0.32
			ACT-8BIN	-	-17	-67	-	0.43	0.36
			ACT-12BIN	187	-8	4	0.72	0.63	0.48
			ACT-20BIN	178	31	25	0.74	0.70	0.51

Table 9. Summary statistics for CN3 and CN10 when using the ACT parameterization in a sectional framework with different numbers of particle size bins. The observed mean, normalized mean bias (NMB) and correlation coefficient (R) are calculated between simulated and observed number concentration collected during the CARES G-1 aircraft flights.

PNC	Flights	Observed mean	NMB(%)		R	
			ACT-12BIN	ACT-20BIN	ACT-12BIN	ACT-20BIN
CN3	June 8, morning (08a)	20472	151	157	0.68	0.64
	June 8, afternoon (08b)	13990	223	274	0.75	0.84
	June 10, morning (10a)	17392	141	212	0.21	0.22
	June 12, morning (12a)	12340	112	198	0.35	0.40
	June 12, afternoon (12b)	14459	175	184	0.11	-0.06
	June 14, morning (14a)	21913	213	259	0.61	0.56
	June 15, morning (15a)	24800	242	250	0.64	0.68
	June 15, afternoon (15b)	14800	275	260	0.73	0.75
	All flights	17564	194	226	0.37	0.52
CN10	June 8, morning (08a)	11588	19	90	0.62	0.57
	June 8, afternoon (08b)	10161	165	162	0.74	0.80
	June 10, morning (10a)	10804	89	95	-0.11	-0.03
	June 12, morning (12a)	6019	61	69	0.39	0.44
	June 12, afternoon (12b)	7940	131	128	-0.02	-0.05
	June 14, morning (14a)	11999	219	221	0.72	0.72
	June 15, morning (15a)	13601	230	216	0.68	0.71
	June 15, afternoon (15b)	12625	260	230	0.73	0.48
	All flights	10641	169	162	0.38	0.54

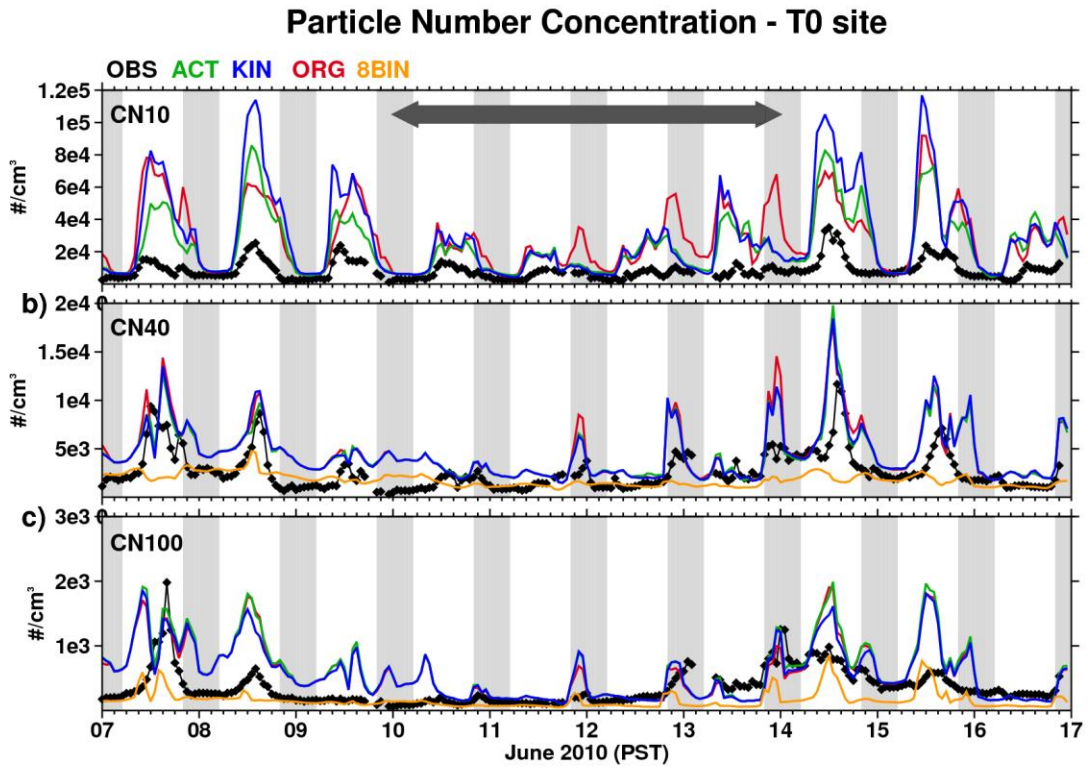

Figure 1. Observed and simulated time series of particle number concentration at the T0 site for a) CN10; b) CN40; c) CN100. Gray shading indicates nighttime and the arrow denotes the period of northerly synoptic flow associated with the passage of a trough over California. All times are local Pacific Standard Time (PST).

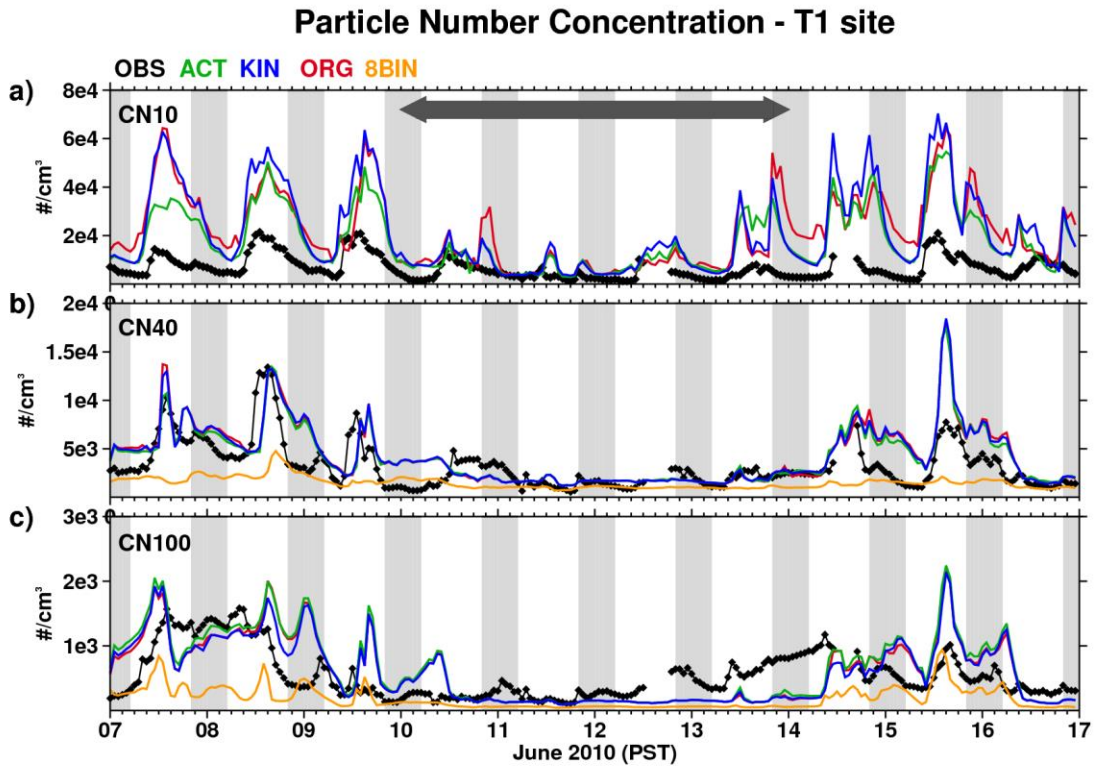

Figure 2. Same as Fig.1, except for the T1 site.

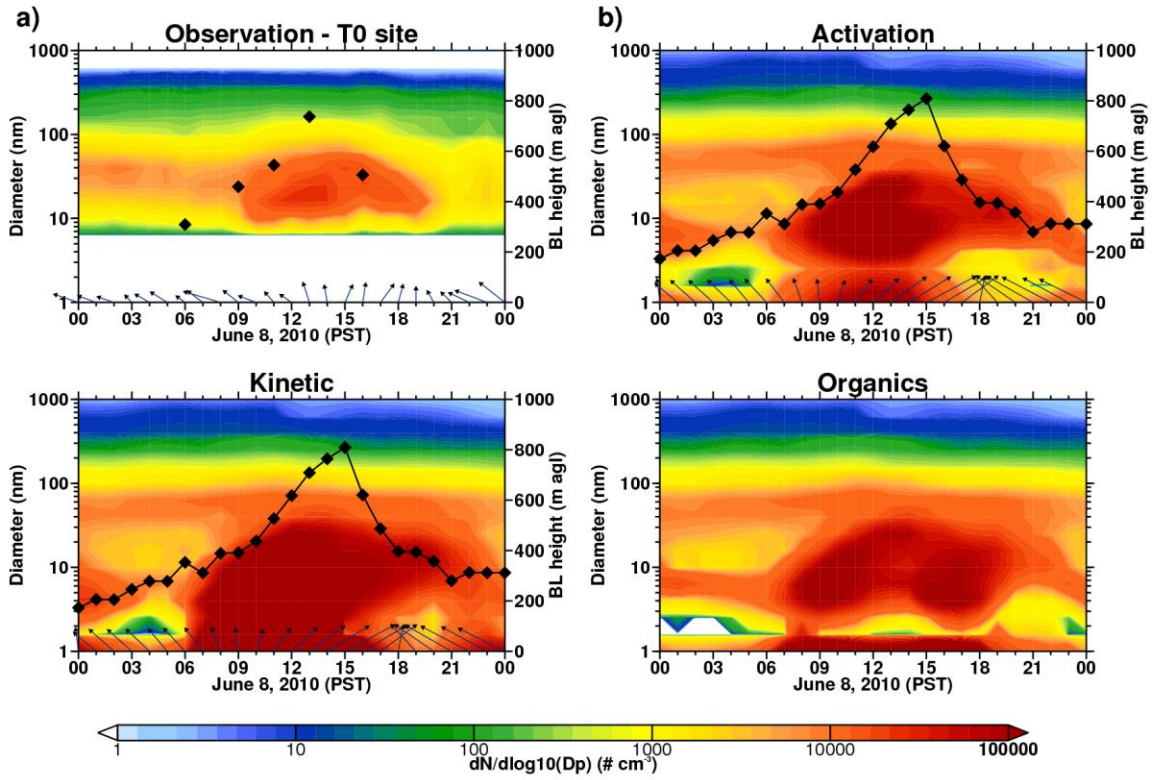

Figure 3. Number size distribution as a function of geometric diameter and time at the T0 site on June 8, 2010 and from a) observations and the b) ACT, c) KIN, and d) ORG simulations. The vectors along the bottom of each panel represent the observed and calculated winds at 10 m above ground level (agl) at the T0 site. The maximum wind speed at about 1500 PST in b)-d) is 6 m s^{-1}. The black diamonds represent the observed (a) and simulated (b-d) boundary layer heights.

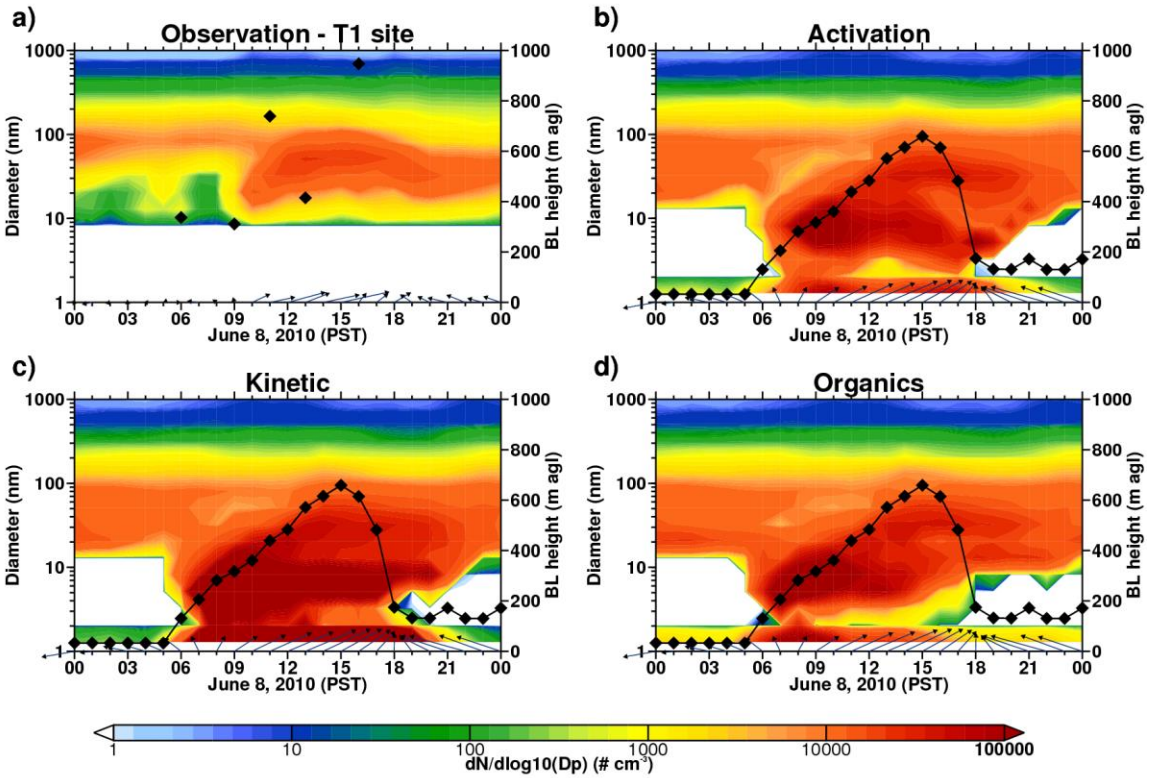

Figure 4. Same as Fig. 3, except for the T1 site.

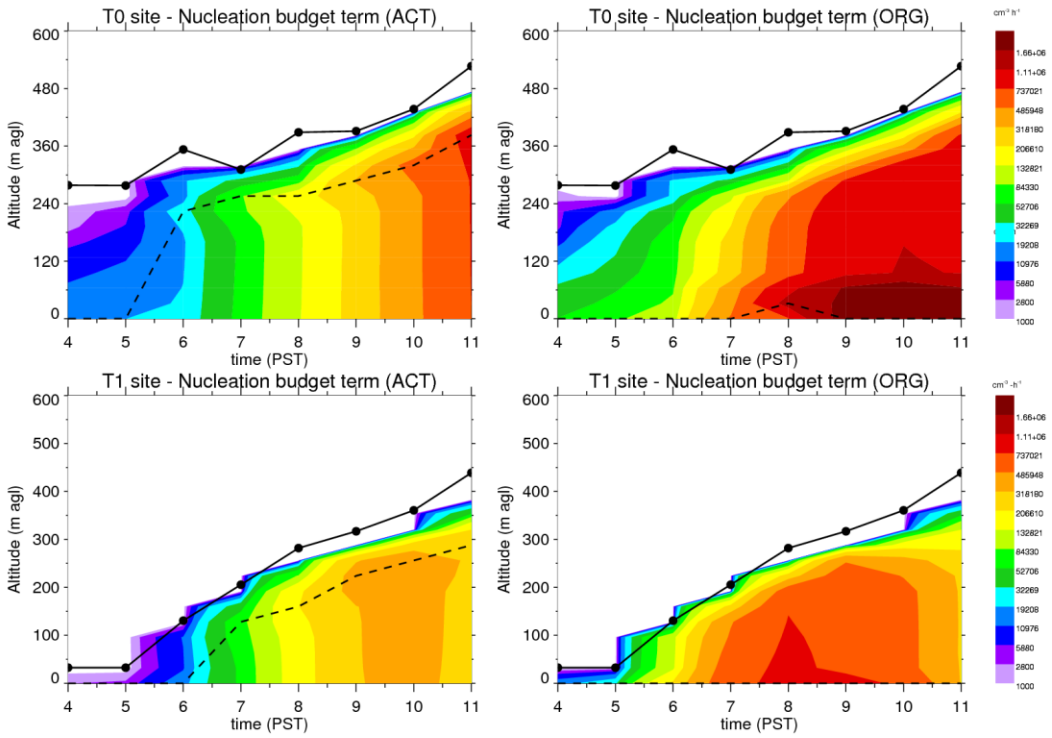

Figure 5. Particle production from the ACT and ORG parameterizations at the T0 and T1 sites on June 8, 2010 together with modeled BL height (circled line). The dashed line shows the altitude of maximum predicted number of small particles.

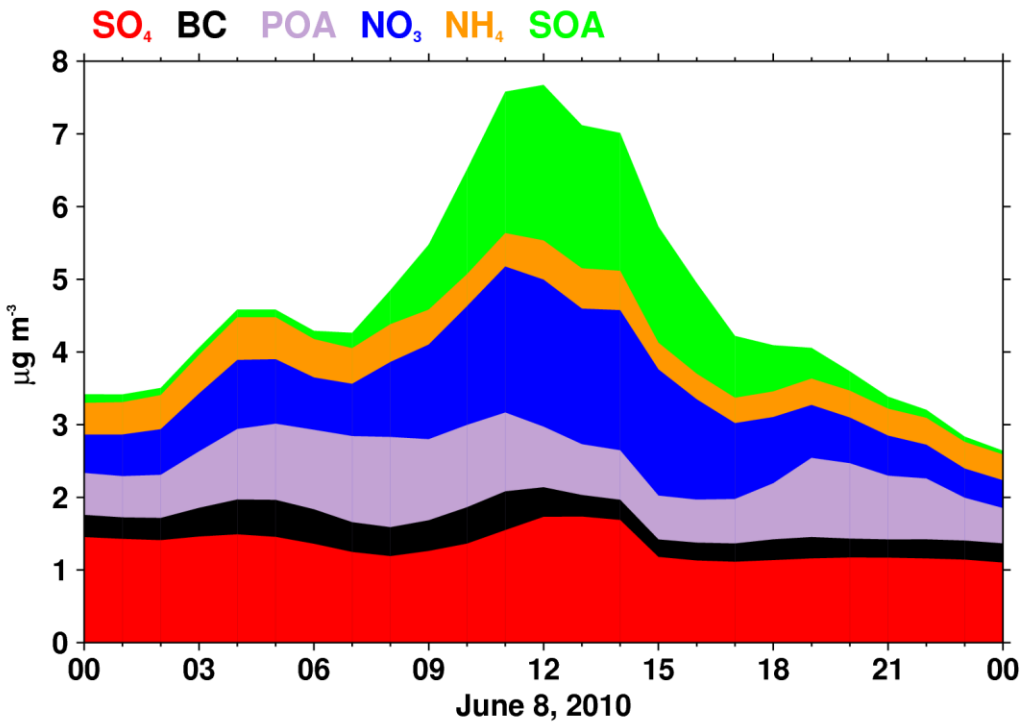

Figure 6. Simulated aerosol mass concentrations at the T0 site on June 8, 2010 predicted by the ACT parameterization.

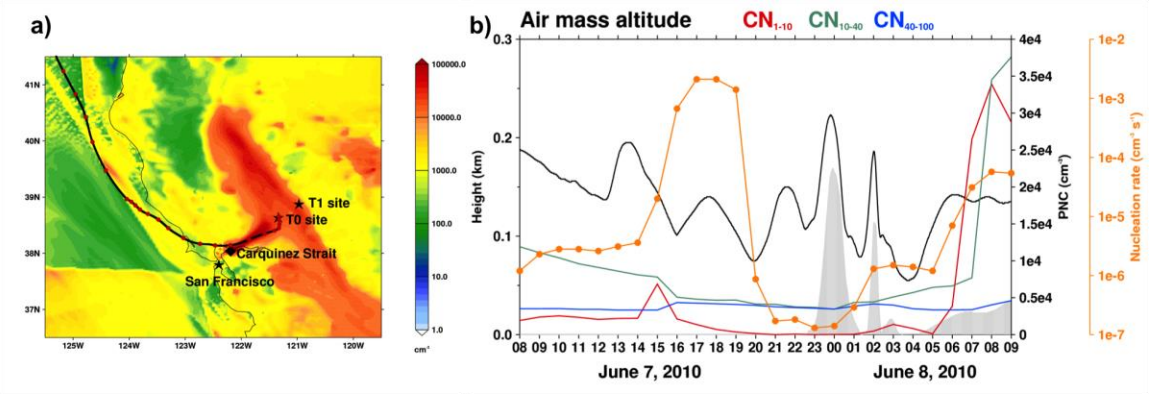

Figure 7. a) Nucleation budget term ($cm^{-3}\,h^{-1}$) averaged over first five model layers from 0500 PST to 0900 PST June 8, 2010 from the ACT simulation, together with a backward trajectory from 0800 PST on June 7 to 0900 PST on June 8, 2010; the red dots denote the hourly locations of the air mass prior to its arrival at the T0 ; b) Altitude of the air mass (black line) together with particle number concentration in 1-10 nm diameter range (red line), 10-40 nm range (green line), 40-100 nm range (blue line) and nucleation rate (orange circled line); the gray area denotes the terrain height.

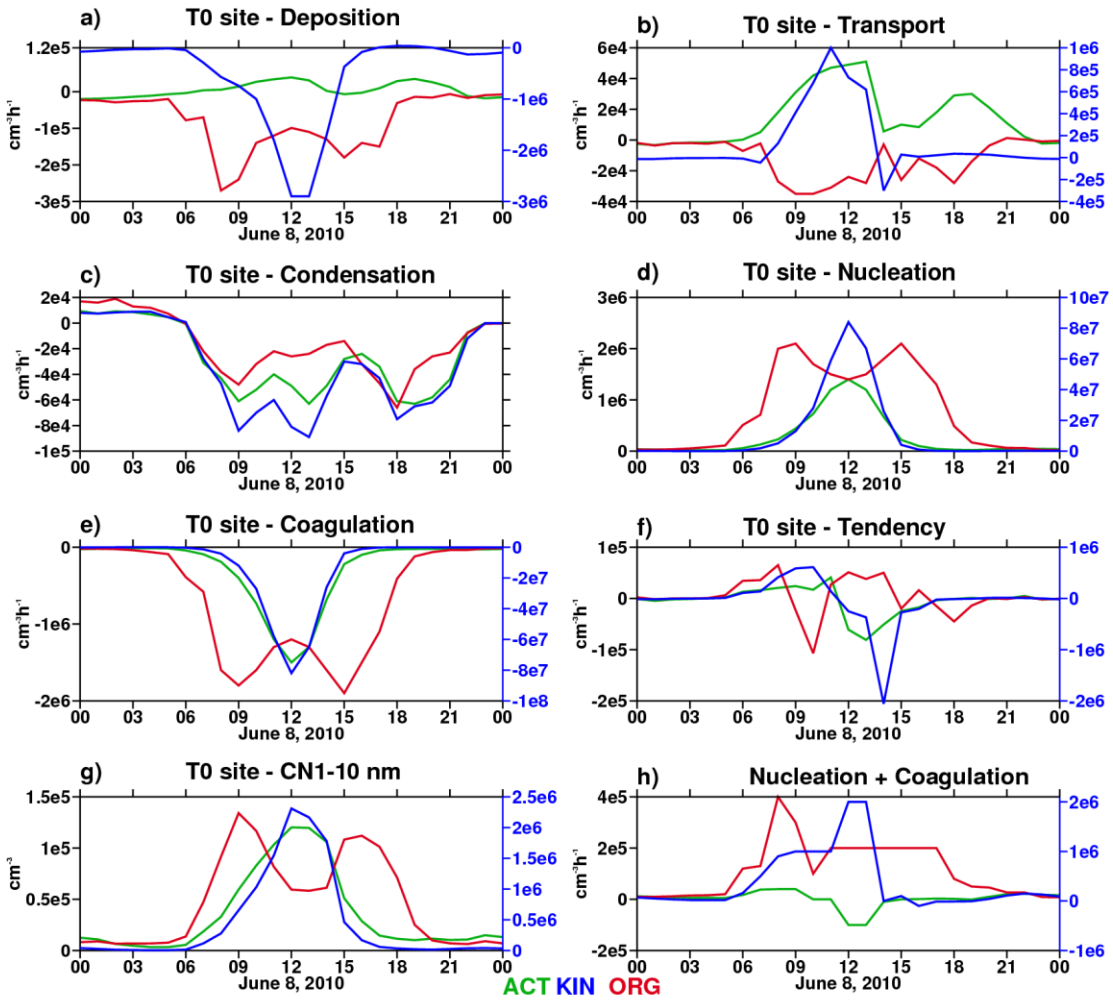

Figure 8. Budget diagnostic terms for 1-10 nm particles at the T0 site on June 8: a) dry deposition; b) transport; c) condensation; d) nucleation; e) coagulation; f) total tendency; g) particle number concentration; and h) tendency of particles coming from nucleation and coagulation processes. The left-hand side (black) vertical axes are for ACT and ORG. The right-hand side (blue) axes are for KIN, which gave larger budget terms.

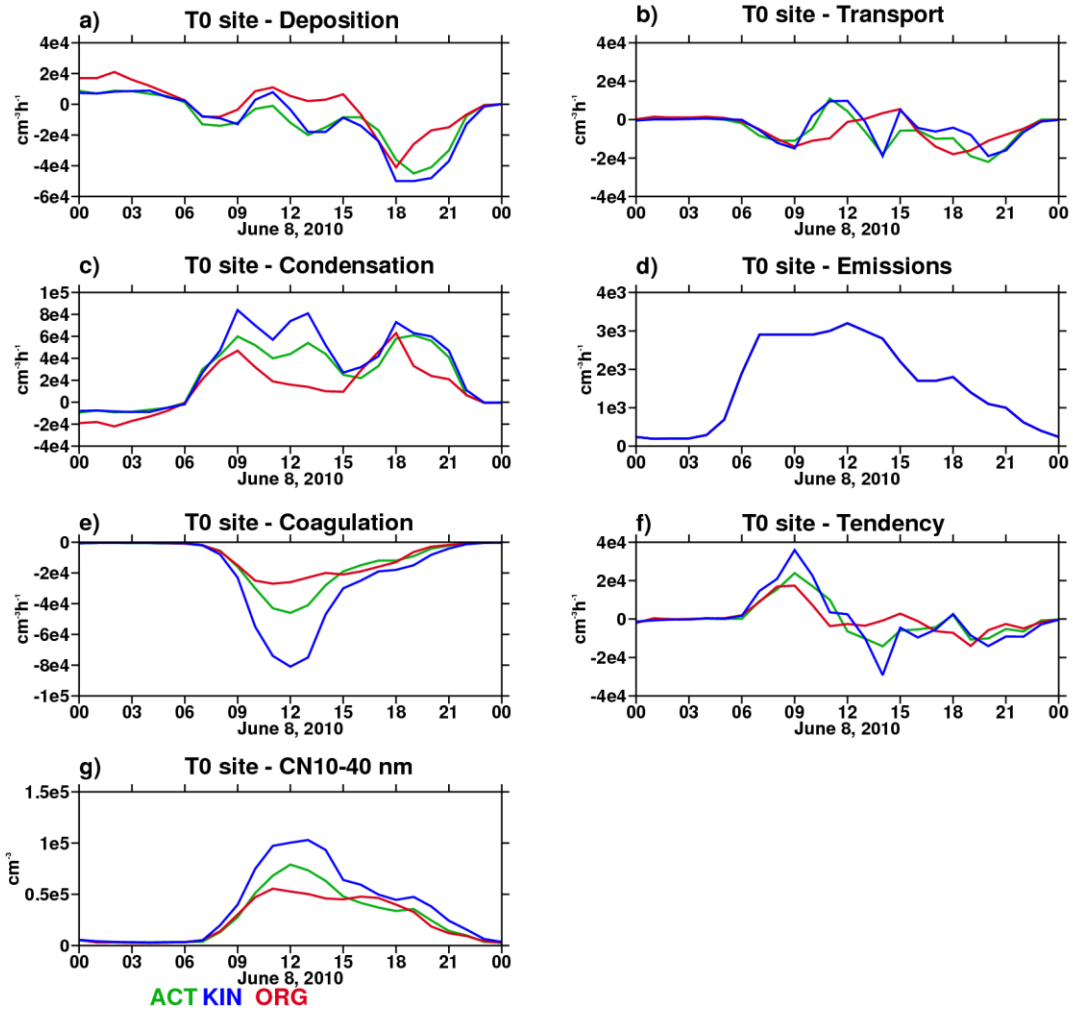

1

2 Figure 9. Budget diagnostic terms for 10-40 nm particles at the T0 site on June 8: a)
3 deposition; b) transport; c) condensation; d) emissions; e) coagulation; f) total tendency;
4 and g) particle number concentration.

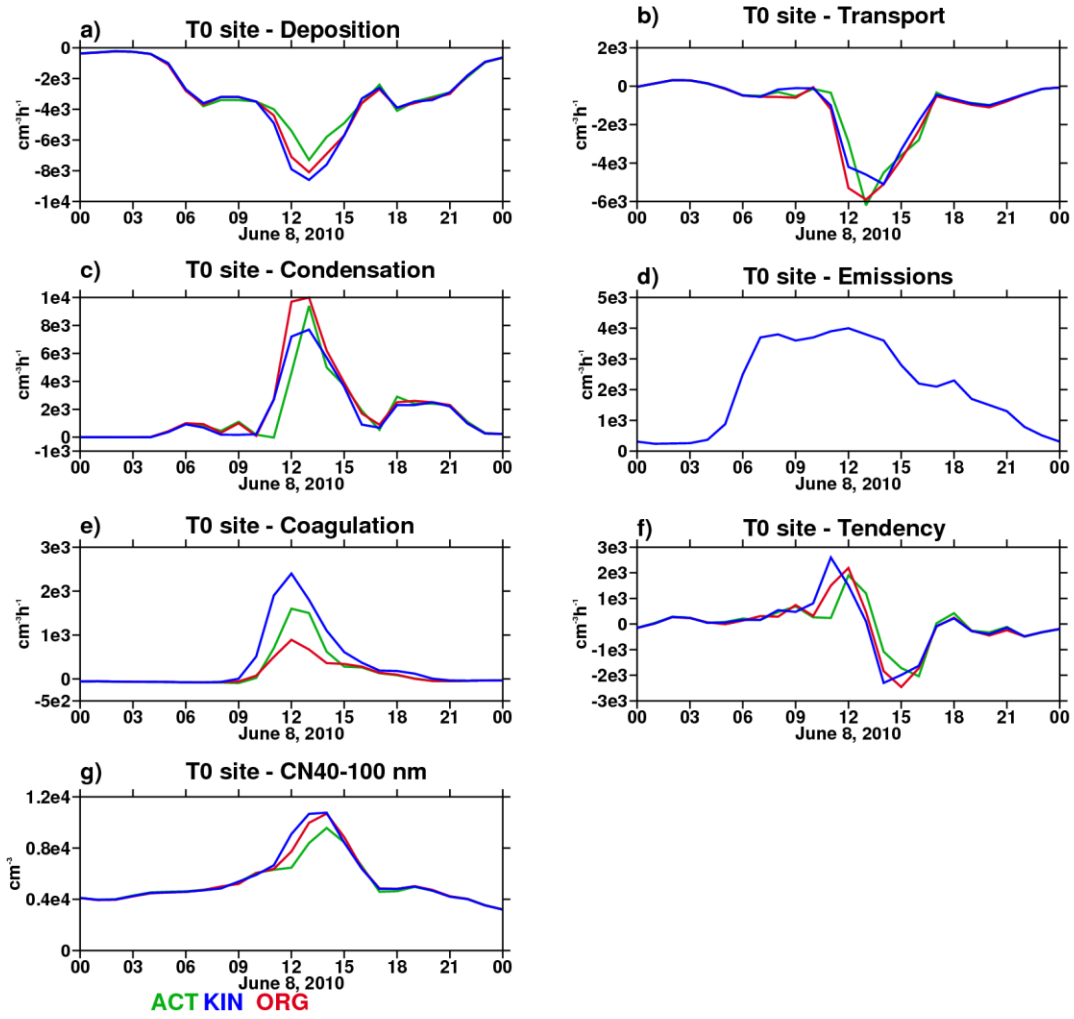

1

2 Figure 10. Budget diagnostic terms for 40-100 nm particles at the T0 site on June 8: a)
3 deposition; b) transport; c) condensation; d) emissions; e) coagulation; f) total tendency;
4 and g) particle number concentration.

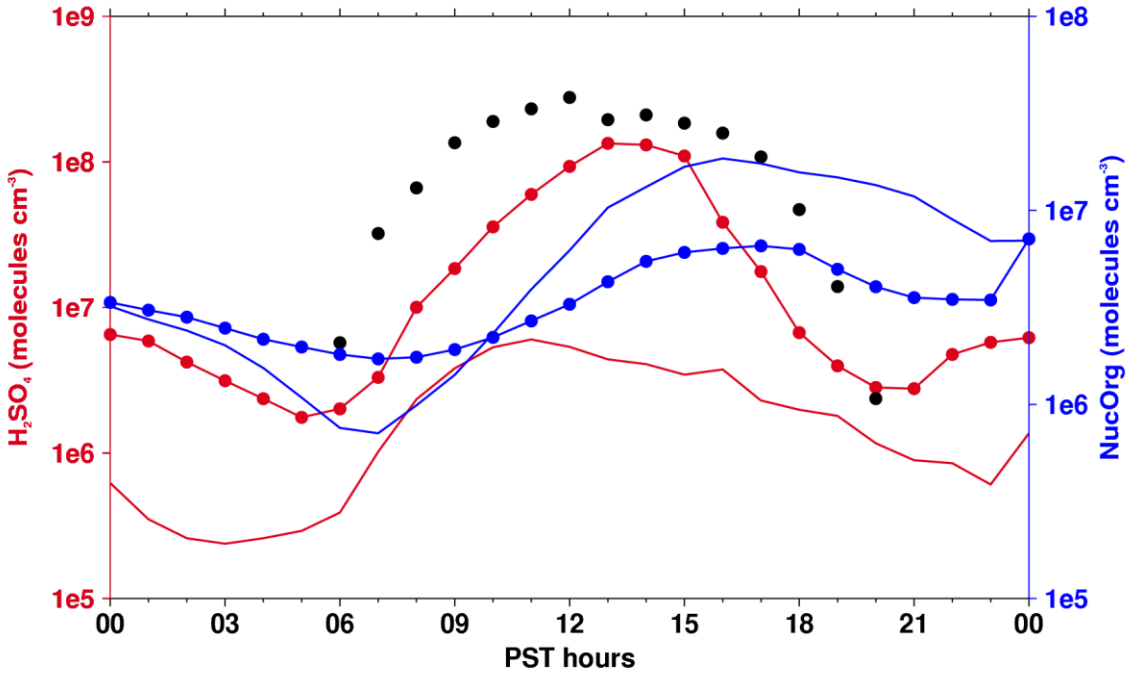

Figure 11. Modeled H_2SO_4 (red lines), and NucOrg concentrations (blue lines) at the T0 site on June 8, 2010 (lines with circles) and June 12, 2010 (lines without circles). The black dots represent the calculated H_2SO_4 proxy on June 8, 2010. The H_2SO_4 proxy is not shown on June 12, 2010 due to missing measurements of SO_2.

1

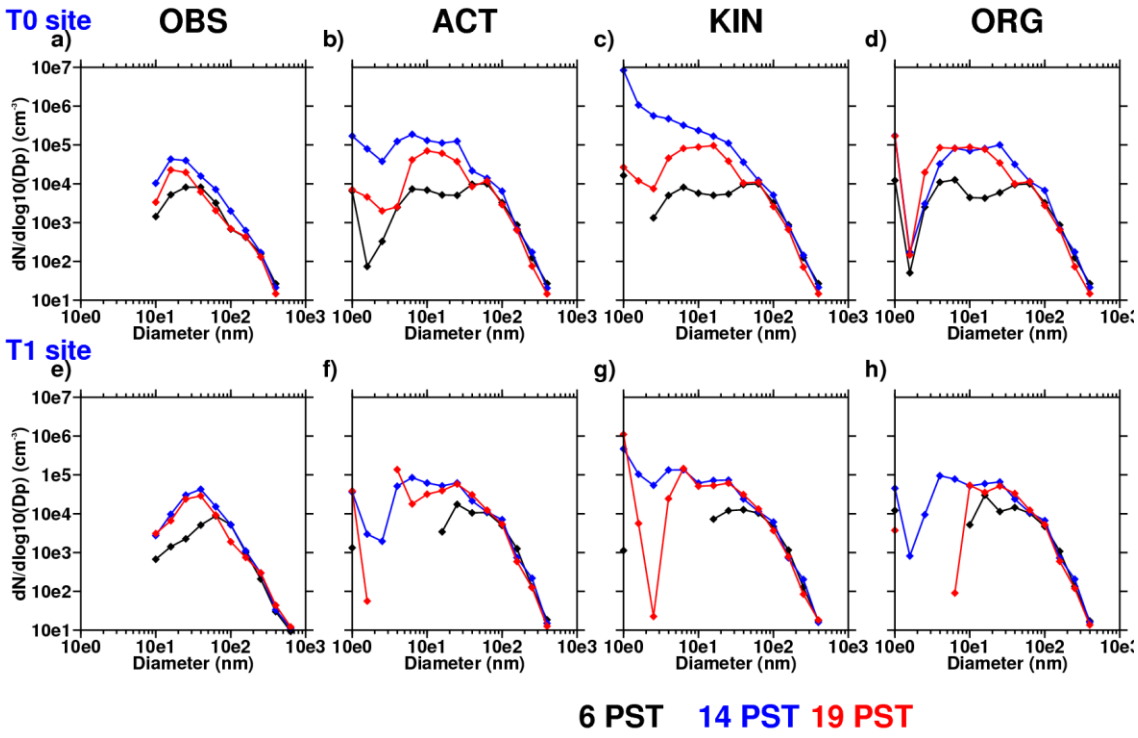

2

3 Figure 12. Particle number distribution for observations (OBS) and the ACT, KIN, and
4 ORG simulations at the T0 (a, b, c, and d) and T1 (e, f, g, and h) sites at 1000 PST (black
5 line), 1400 PST (blue line) and 1900 PST (red line) on June 8, 2010. The missing line
6 segments in the simulations correspond to particle number lower than 10 cm^{-3}.

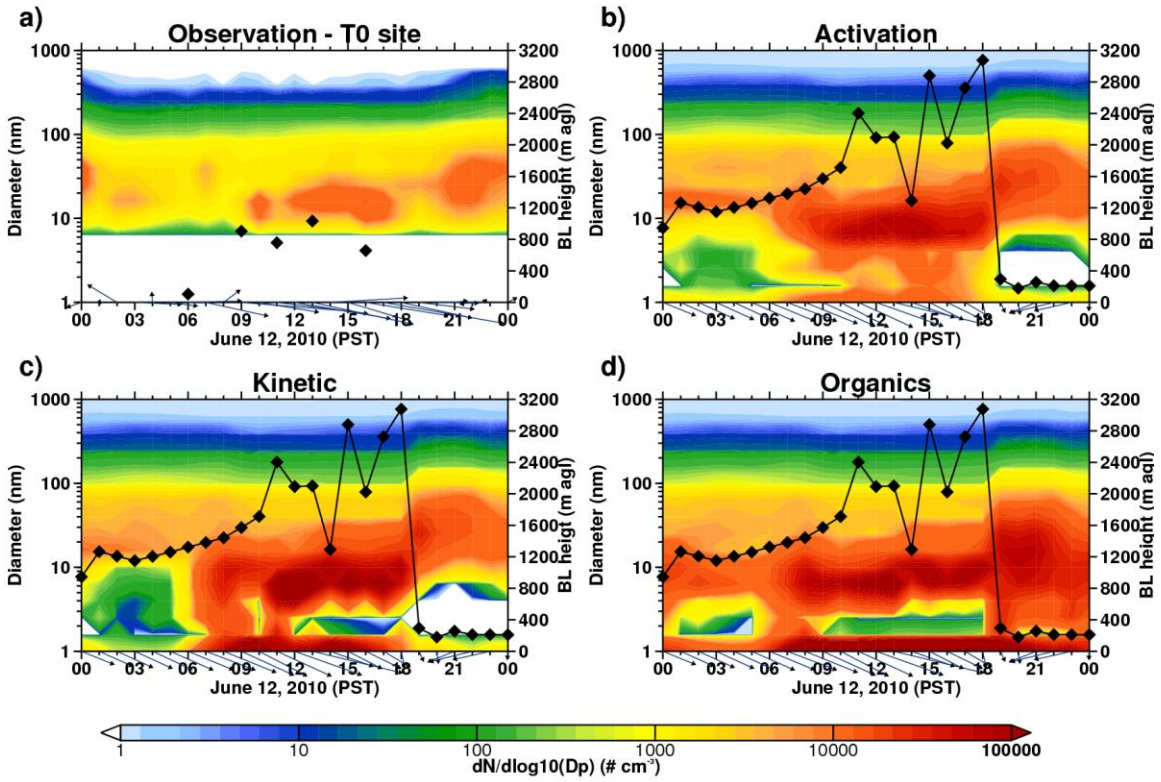

Figure 13. Number size distribution as a function of geometric diameter and time at the T0 site on June 12, 2010 from a) observations and the b) ACT, c) KIN, and d) ORG simulations. The vectors along the bottom of each panel represent the observed and calculated winds at 10 m AGL at the T0 site. The maximum wind speed at about 1200 PST in b)-d) is 10.4 m s^{-1}. The black diamonds represent the observed (a) and simulated (b-d) boundary layer heights.

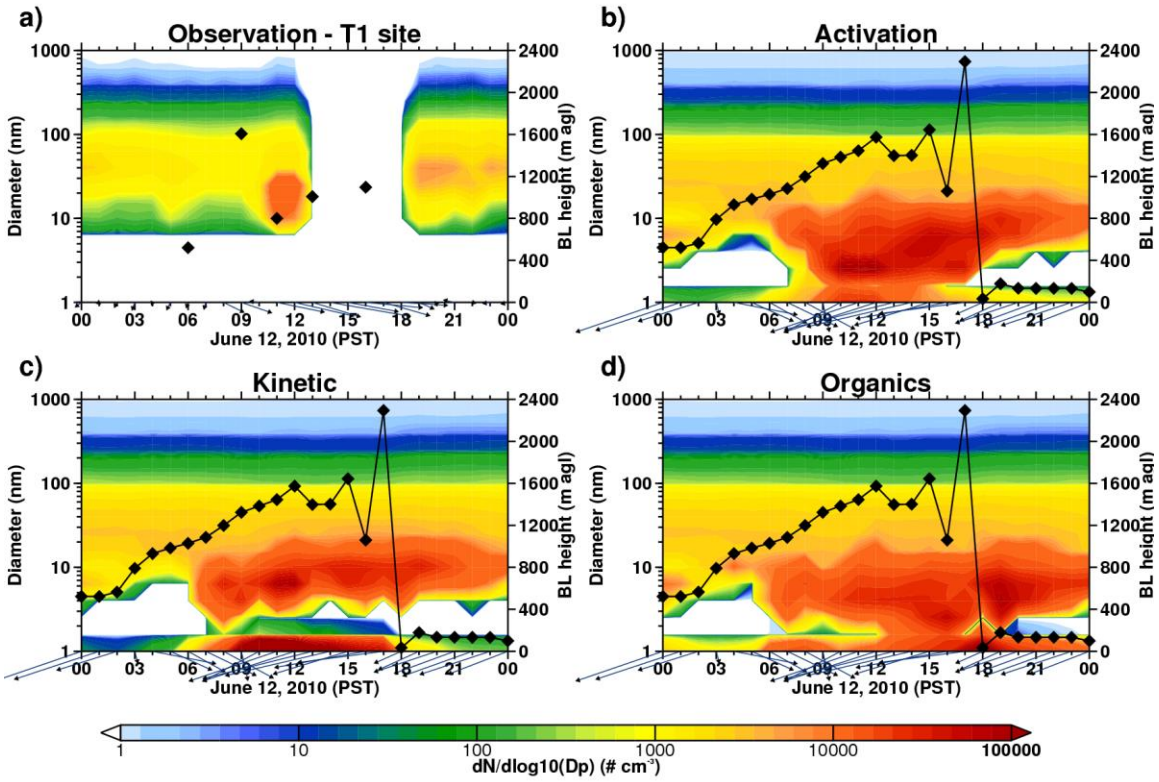

Figure 14. Same as Fig. 13, except for the T1 site.

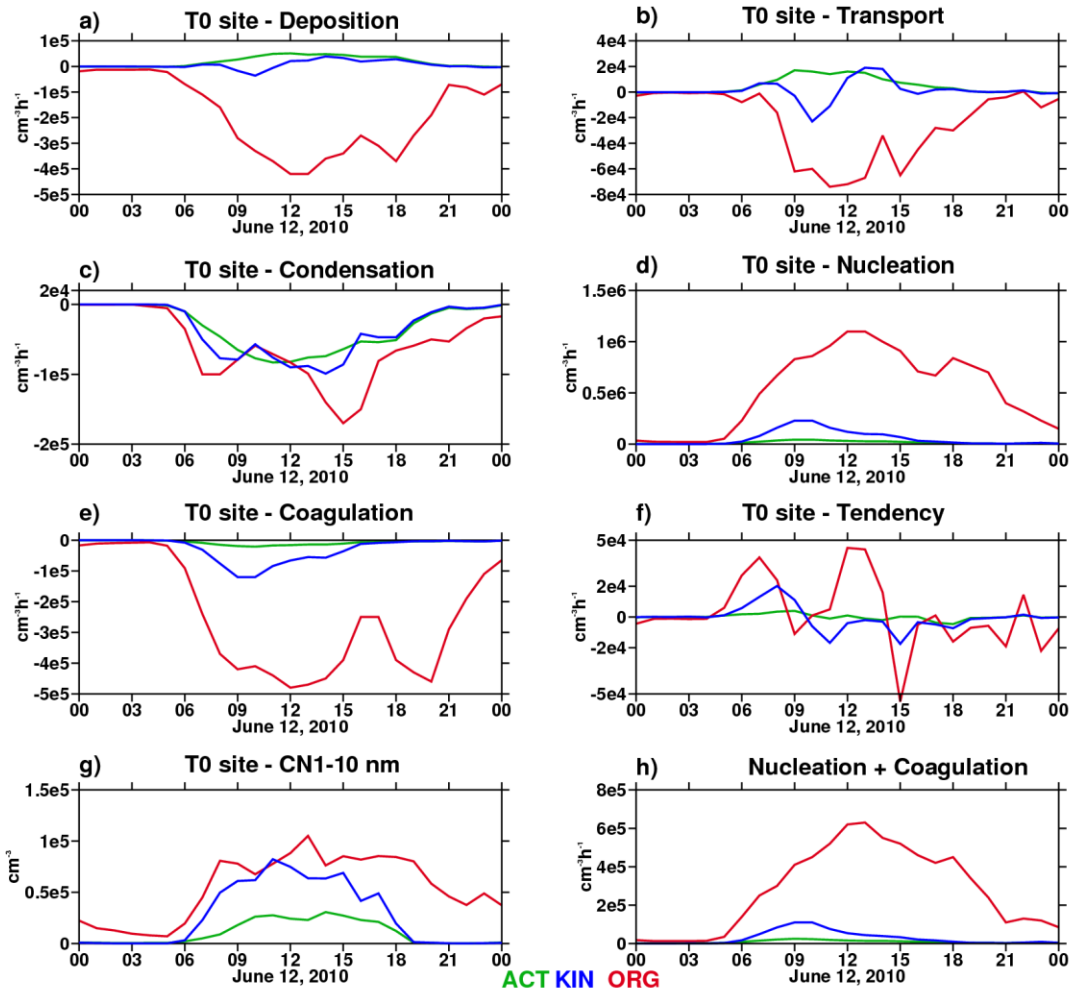

Figure 15. Budget diagnostic terms for 1-10 nm particles at the T0 site on June 12: a) deposition; b) transport; c) condensation; d) nucleation; e) coagulation; f) total tendency; g) particle number concentration in 1 to 10 nm range; and h) tendency of particles coming from nucleation and coagulation processes.

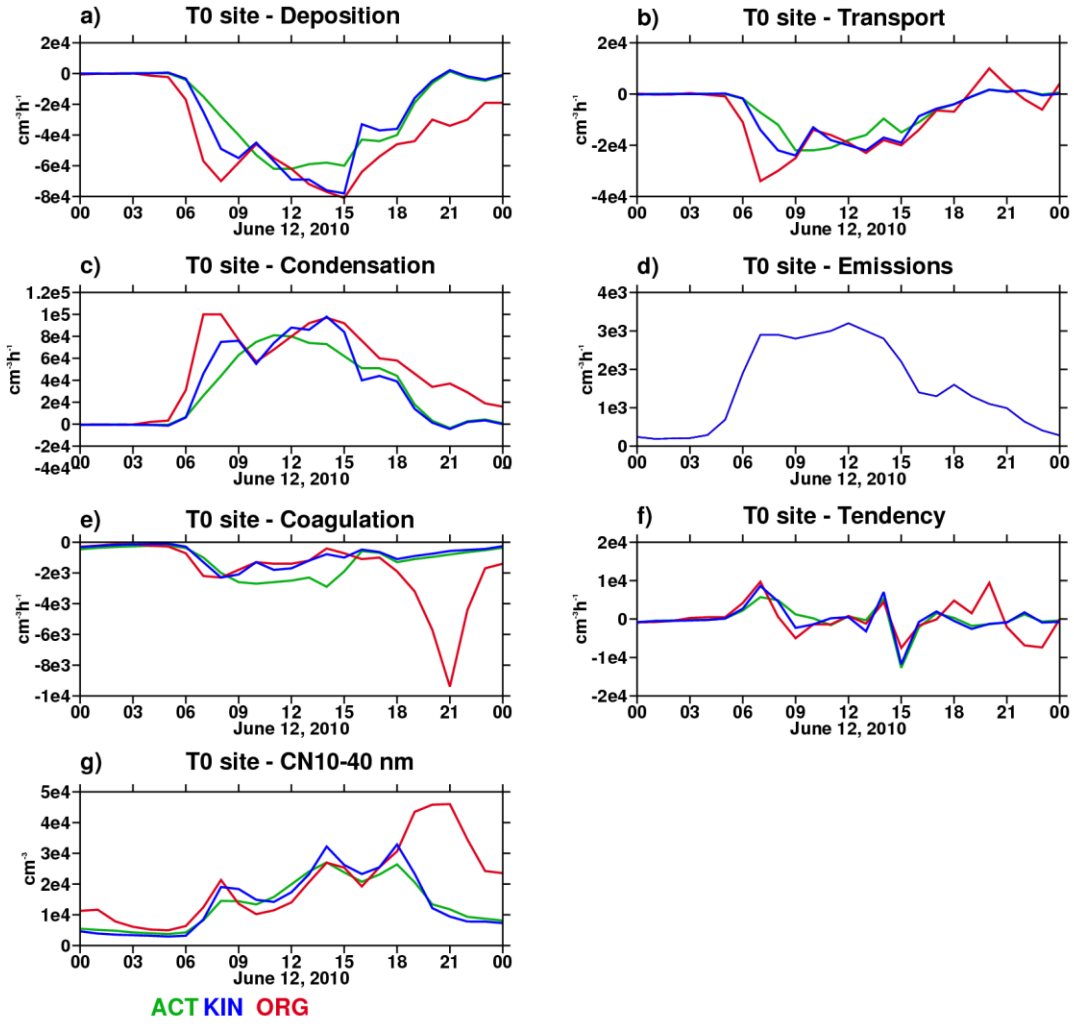

1

2 Figure 16. Budget diagnostic terms for 10-40 nm particles at the T0 site on June 12: a)
3 deposition; b) transport; c) condensation; d) emissions; e) coagulation; f) total tendency;
4 and g) particle number concentration.

5

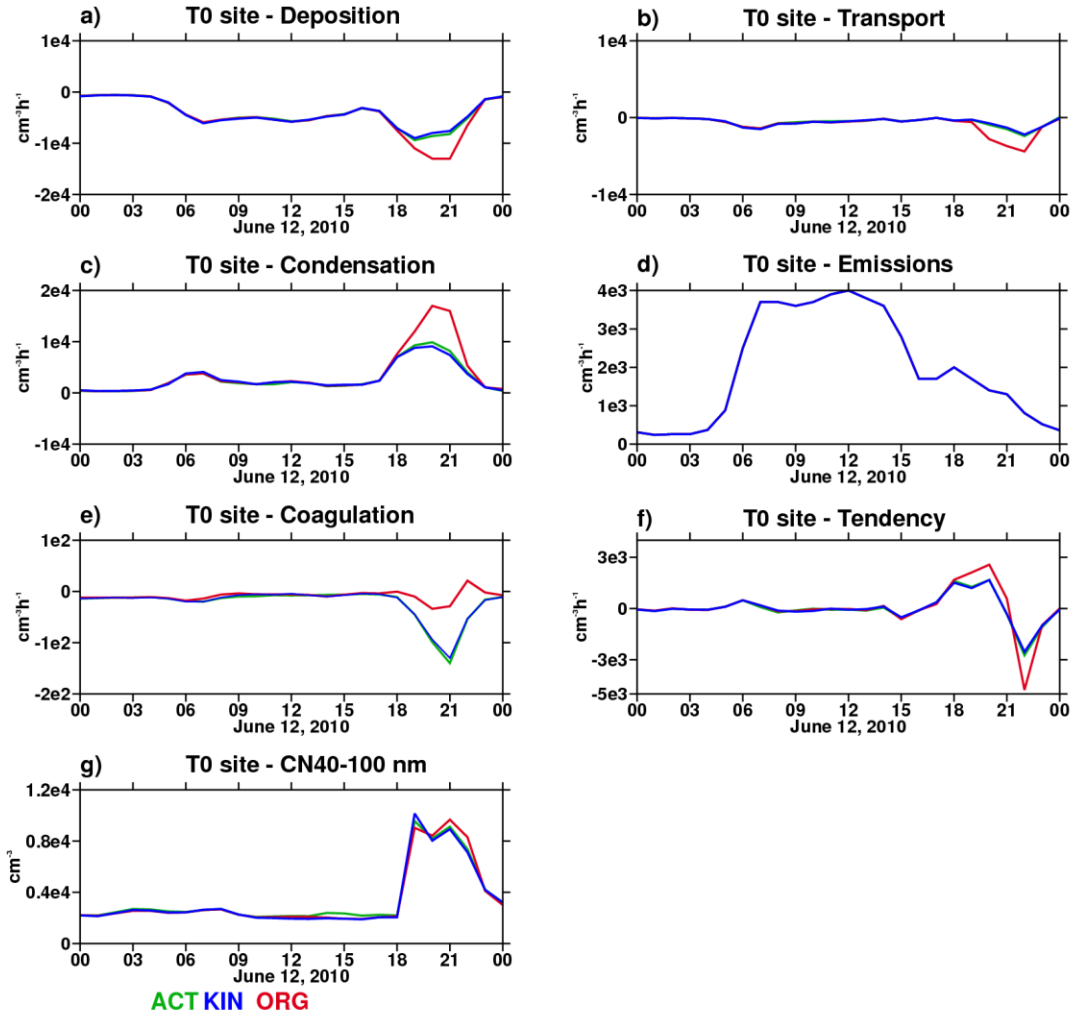

Figure 17. Budget diagnostic terms for 40-100 nm particles at the T0 site on June 12: a) deposition; b) transport; c) condensation; d) emissions; e) coagulation; f) total tendency; and g) particle number concentration.

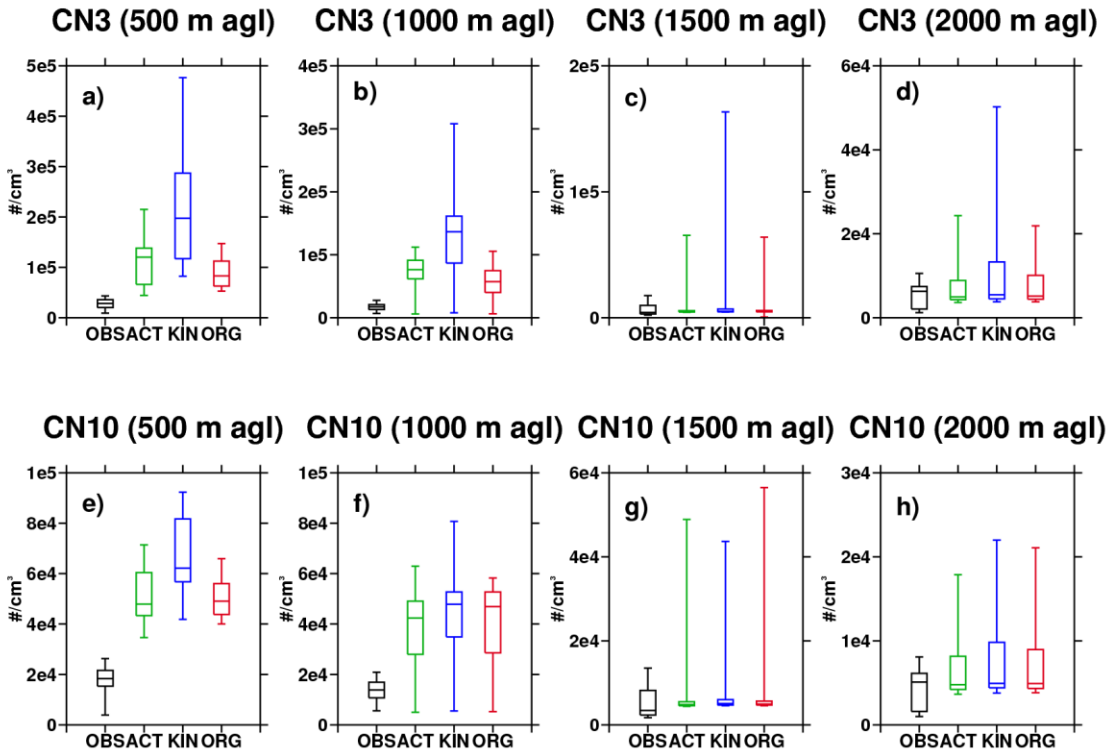

Figure 18. Boxplot for observed and simulated CN3 and CN10 at the surface to 500 m altitude [a) and e)]; 500-1000 m altitude [b) and f)] 1000-1500 m altitude [c) and g)]; and 1500-2000 m altitude [d) and h)] for the June 8, 2010 afternoon G-1 flight. Observations are in black, ACT simulation values are in green, KIN in blue, and ORG in red. The line in the middle of each box is the median, while the boxes represent the 25th and 75th percentiles, and "whiskers" the 5th and 95th percentiles.

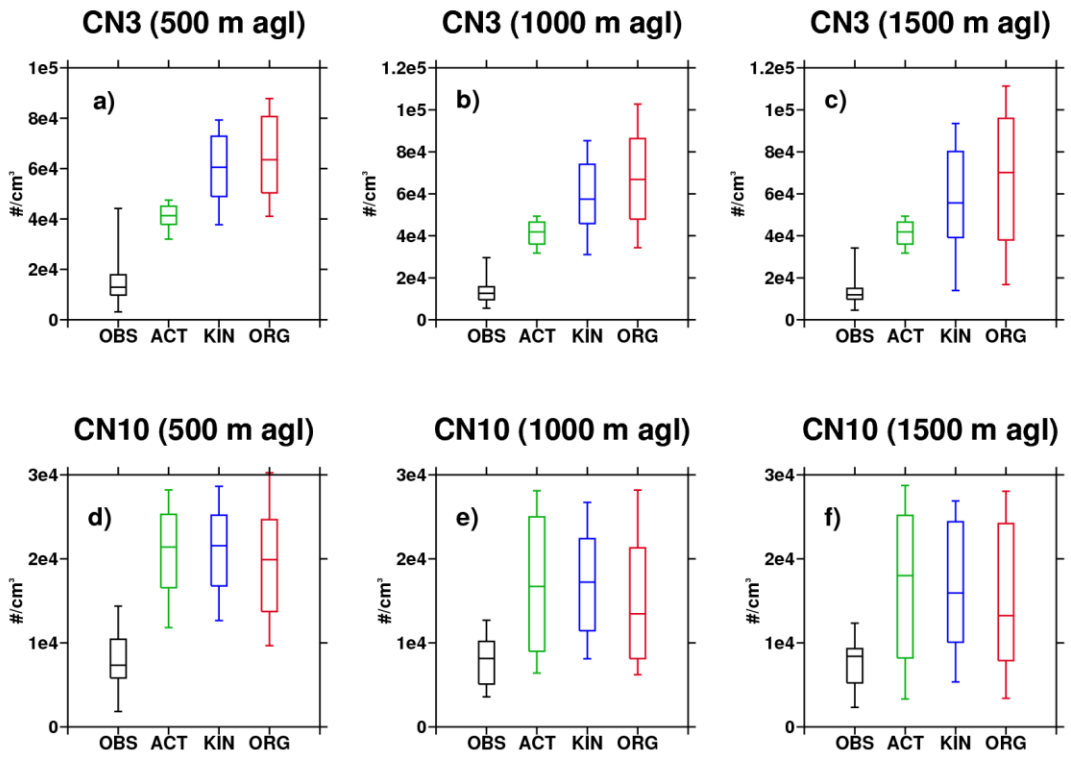

Figure 19. Same as Fig. 18, except for the June 12, 2010 afternoon G-1 flight.

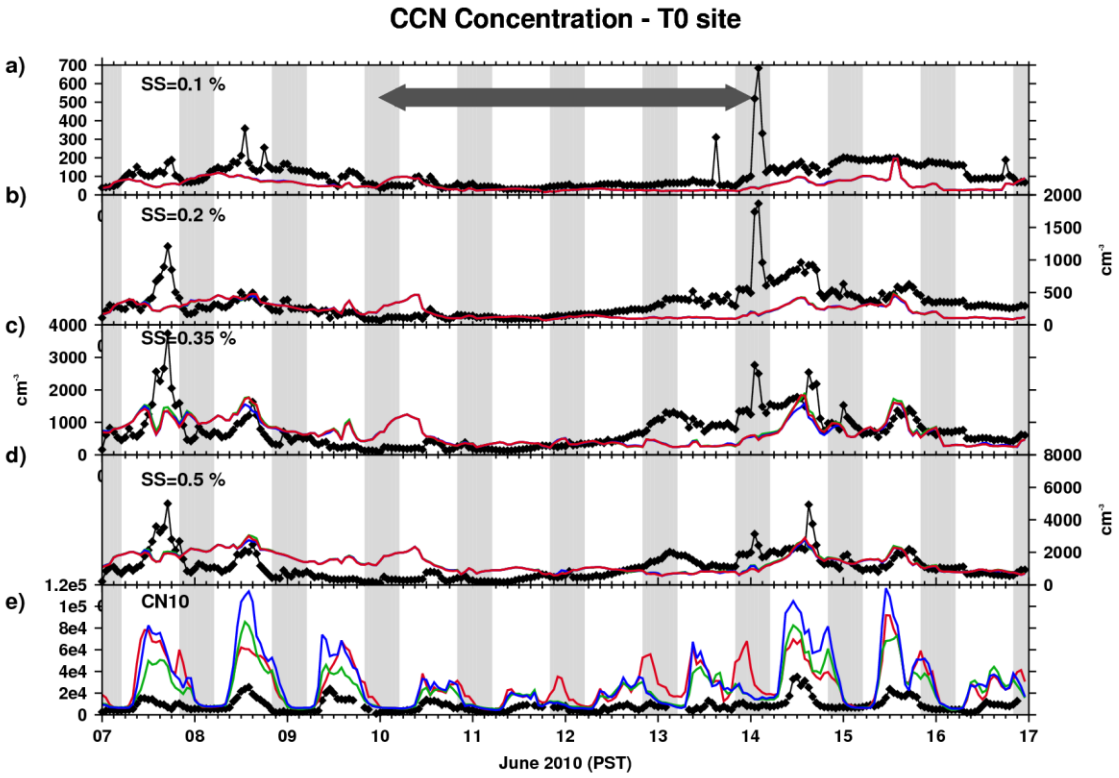

Figure 20. Observed and simulated time series of CCN number concentration at the T0 site for a) SS=0.1%; b) SS=0.2%; c) SS=0.35% e) SS=0.5% together with e) CN10 concentration. Gray shading area indicates nighttime while the black arrow denotes the northerly synoptic flow associated with the passage of troughs over California.

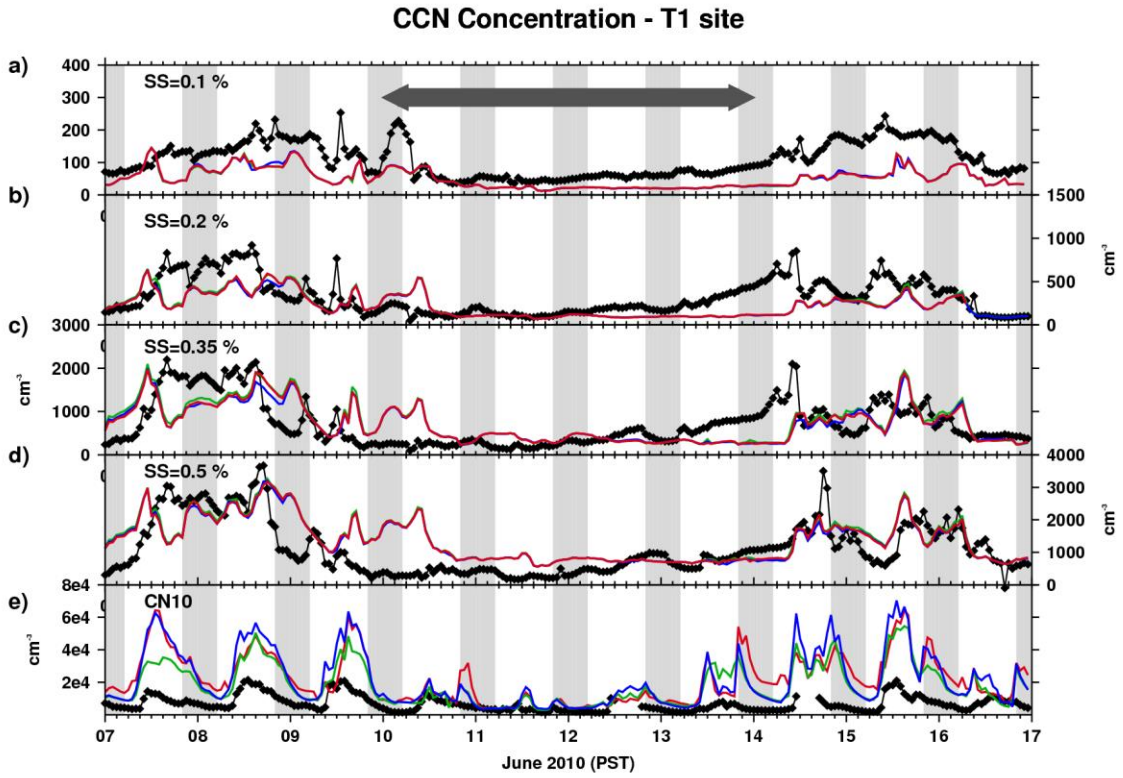

Figure 21. Same as Fig. 20, except for the T1 site.